Ann. Geophys., 44, 855–880, 2026
https://doi.org/10.5194/angeo-44-855-2026
© Author(s) 2026. This work is distributed under
the Creative Commons Attribution 4.0 License.

Annales Geophysicae Open Access EGU

Dune aurora: survey from a citizen science database

Maxime Grandin[1], Liisa Juusola[1], Noora Partamies[2], Emma Bruus[3,4], Joona Rautiainen[3], Donna Lach[5], Jia Jia[1], Max van de Kamp[1], Eero Karvinen[4], Kirsti Kauristie[1], and Theresa Hoppe[1]

[1]Finnish Meteorological Institute, Helsinki, Finland
[2]Department of Arctic Geophysics, The University Centre in Svalbard, Longyearbyen, Norway
[3]Sodankylä Geophysical Observatory, University of Oulu, Sodankylä, Finland
[4]Skywarden observation system, Ursa Astronomical Association, Helsinki, Finland
[5]Aurorasaurus, New Mexico Consortium, Los Alamos, NM, USA

Correspondence: Maxime Grandin (maxime.grandin@fmi.fi)

Received: 31 October 2025 – Discussion started: 16 December 2025
Revised: 20 May 2026 – Accepted: 12 August 2026 – Published: 27 August 2026

Abstract. Auroral forms can provide information not only on the state of near-Earth space but also on conditions in the lower-thermosphere–ionosphere. The so-called dune aurora, consisting of brighter stripes forming a wave-like pattern in the dim, diffuse green aurora, has been hypothesised as being an optical signature revealing the presence of large-scale atmospheric waves above or near the mesopause. However, only a few dune aurora events have been studied to date, leaving many open questions regarding the nature of this phenomenon. We carry out the first systematic survey of dune aurora events by collecting citizen science observations of the dunes since 2000 using the Skywarden (https://taivaanvahti.fi, last access: 25 August 2026) database of observations. From a total of 308 dune aurora observations made during 61 different events by citizen scientists from Northern Europe, North America, Australia, and New Zealand, we investigate the distribution of dune events as a function of location, month, magnetic local time (MLT), solar wind and interplanetary magnetic field (IMF) conditions, and geomagnetic activity. We compare those distributions to that of all the aurora observations reported in Skywarden since 2000. We find that the vast majority (92 %) of the dune reports were made by observers below 61° geomagnetic latitude (to be compared to 74 % for all aurora observations), suggesting that they frequently occur in the equatorward part of the auroral oval. The dune observations are mostly (89 %) made in the pre-midnight sector, with a peak between 21:00 and 22:00 MLT (between 23:00 and 00:00 MLT for all aurora observations). The months with the highest number of reports of dune observations are October and March, which could be the result of a combination of geomagnetic, atmospheric, darkness, and cloudiness conditions needed for them to be observed. Regarding the solar wind and IMF driving parameters, no statistically significant differences are found between dune and all-aurora observations, but the differences are significant for geomagnetic indices, with dune observations being made during more active conditions than for all types of aurora considered together. Finally, we investigate a possible relationship between dune aurora and equivalent current patterns derived from ground-based magnetometer measurements. We find that, for all the reported events, the dunes are observed in association with strong (in most cases eastward but occasionally westward) auroral electrojet signatures and in the vicinity of the Harang discontinuity. These results suggest that the dune aurora formation mechanism might involve an interplay between proton precipitation, atmospheric dynamics, and nightside transition region processes.

1 Introduction

The interplay between the upper atmosphere and space is complex and remains to a great extent poorly understood. The lower-thermosphere–ionosphere is subject to forcing from space via, for instance, charged particle precipitation, electric currents flowing within the ionosphere–magnetosphere system, and high-latitude plasma drifts associated with magnetospheric convection (e.g. Palmroth et al.,

2021; Sarris et al., 2023). This region is also affected by the underlying atmospheric layers from which upward propagating waves contribute to the neutral gas dynamics (e.g. Vadas and Liu, 2009; Vadas and Becker, 2019; Heelis and Maute, 2020). As measuring the properties of the lower-thermosphere–ionosphere is challenging, one way to indirectly obtain information on its state is to observe optical emissions coming from it. It has been shown, for instance, that the STEVE (Strong Thermal Emission Velocity Enhancement) phenomenon (MacDonald et al., 2018) is the optical signature of subauroral ion drifts (SAID; Archer et al., 2019), which are narrow channels of fast-flowing plasma in the thermosphere, difficult to measure in the absence of in situ satellite observations.

Another form of optical emission of particular interest to reveal upper-atmospheric dynamics is the dune aurora, which has also been referred to as "the dunes". The dunes are a diffuse auroral form exhibiting a wave pattern such that it forms bands of increased brightness roughly parallel to each other (see an example in Fig. 1). Like STEVE, the dunes were discovered thanks to citizen scientists. Using two pictures of the same dune display taken almost exactly at the same time, Palmroth et al. (2020) could determine that the auroral emission associated with the dunes was produced at approximately 100 km altitude, and that the region where they took place corresponded to that of the eastward electrojet. In a subsequent study, Grandin et al. (2021) found that dune aurora could span over 1500 km of horizontal distance (from western Finland to Scotland) and be visible for at least four hours. That study also revealed that the dunes were associated with 10–20 keV electron precipitation and a large temperature inversion layer below the mesopause. A possible role of precipitating protons was also discussed in that study, though more investigation is needed to examine their potential importance in the formation of dune aurora. In the few events that have been studied, the dune stripes exhibit a pseudo-wavelength ranging between 30 and 45 km (Palmroth et al., 2020; Grandin et al., 2021) and have an orientation roughly perpendicular to the auroral oval, although it is unclear whether this is always the case. In Grandin et al. (2021), the dunes were found to propagate at about 200 m s^{-1} with respect to the observer on the ground, in the westward direction.

The above elements suggest that the dunes may be the optical signature of an atmospheric wave propagating horizontally within diffuse aurora near the mesopause, as hypothesised in Palmroth et al. (2020). A candidate for such a wave could be the mesospheric bore (Dewan and Picard, 1998; Smith et al., 2003), whose properties (wavelength, propagation speed, altitude) are compatible with the observations reported in Palmroth et al. (2020) and Grandin et al. (2021). Mesospheric bores are known to form and propagate in presence of a ducting structure, which can be a temperature inversion layer in the mesosphere (thermal duct) or a wind shear below the mesopause (Doppler duct), as detailed in Dewan and Picard (2001). They are generally observed in airglow images and have been predominantly studied at low and mid-latitudes (e.g. Hozumi et al., 2019). Their horizontal wavelength can range between 20 and over 100 km (Brown et al., 2004), and they typically have a spatial extent over several hundreds of kilometres. In some cases, a given mesospheric bore can contain over 15 trailing crests and troughs (Su et al., 2018). Recently, Chauhan et al. (2024) carried out a study of high-latitude mesospheric bores whose horizontal wavelengths ranged within 10–50 km for phase speeds within 20–100 m s^{-1}. They found no correlation with auroral activity.

Besides mesospheric bores, it has been suggested that the dunes could be associated with acoustic waves. These would propagate within a non-linear periodic duct produced by meteor showers creating a dusty plasma around 100 km altitude (Izvekova et al., 2025). However, a totally distinct alternative hypothesis to explain the dune aurora's morphology involves a magnetospheric origin, with exohiss waves near the plasmapause spatially modulating the precipitating particle fluxes (He et al., 2023).

In the absence of conclusive evidence to confirm one of the hypotheses, there remain several open questions in relation to the dunes:

1. How frequent are the dunes, and are they associated with specific solar wind driving or geomagnetic activity conditions?

2. What is the distribution of the dune aurora as a function of geomagnetic latitude and magnetic local time (MLT)? Do they appear all year round, or is there a seasonality in their occurrence? What is the typical duration of a dune aurora event?

3. Do precipitating protons play a role in the formation of the dunes?

4. Are the dunes associated with the presence of an atmospheric wave near the mesopause? If so, is the mesospheric bore the most likely candidate wave?

5. Does the morphology of the dune aurora originate from magnetospheric processes?

Since the dunes have so far remained challenging to identify from all-sky camera images, a pathway to better understand them is to involve citizen science observations – that is, reports or photographs made by people who are not researchers by profession. Indeed, the narrower field-of-view of commercial cameras as typically used by aurora photographers is more suitable to reveal their presence in the diffuse aurora, especially since they tend to be more visible when viewed at relatively low elevations where structures in all-sky images are not easy to analyse. Although it is not fully clear why this is the case, possible explanations could involve geometric effects, such as stronger contrast within the

Figure 1. Example of dune aurora. The photograph was taken by Donna Lach on 9 November 2024 from the western shore of Lake Manitoba, Canada. The white rectangle indicates where the dunes are visible.

dune structures when seen off-zenith (due to both larger optical depth and narrower angular width when they are visible at low elevation, making the luminosity gradients more discernable) and the compression of low-elevation auroral structures near the edges of all-sky camera images. Auroral citizen science has recently gained significant momentum (see Grandin et al., 2025, for a recent review), especially boosted by the May 2024 extreme geomagnetic storm (e.g. Spogli et al., 2024; Grandin et al., 2024; Hayakawa et al., 2025; Lockwood et al., 2025).

This study presents the first systematic survey of dune aurora observations combining 308 reports by citizen scientists from all around the world with measurements from scientific instruments. Section 2 describes the data sets and methods used in the study. Section 3 presents the results of the analysis in terms of spatio-temporal distribution of dune observations, their duration, their relation to solar wind driving and geomagnetic activity, and their association with ionospheric currents. Section 4 discusses the results, and conclusions are summarised in Sect. 5.

2 Data and methods

2.1 Citizen science observations from Skywarden

Skywarden (Taivaanvahti in Finnish, Himlakollen in Swedish; https://taivaanvahti.fi, last access: 25 August 2026) is a database of observations of celestial phenomena (aurora, solar halos, deep-sky objects, noctilucent clouds, thunderstorms, eclipses, fireballs …) made by citizen scientists. It has been created, developed and maintained by the Ursa Astronomical Association in Finland. It was established in 2011 but it also includes a handful of historical observations which have been digitised recently; the oldest ones are a series of photographs of the aurora taken in Sodankylä in late 1927 – probably the oldest aurora photographs taken in Finland (Nevanlinna and Tanskanen, 2024). Skywarden has already proved useful as a database for studies investigating proton aurora and stable aurora red arcs (Nishimura et al., 2022) as well as the May 2024 geomagnetic storm (Grandin et al., 2024; Lockwood et al., 2025).

We used the Skywarden application programming interface (API; Bruus, 2024) to search for observations made by citizen scientists during which dunes were identified. We carried out the search between 1 January 2000 and 31 December 2025, and restricted it to observations containing at least one photograph where the dunes were visible. Dune observations were confirmed through three steps:

1. The observers themselves, in most cases, indicated that their pictures contained structures that may be dunes. Some experienced observers are familiar enough with the dunes to reliably identify them in their material, whereas others may be unsure about it but were encouraged to review their observations aided with freely available material providing guidelines for auroral form identifications – both integrated into Skywarden itself and as open material such as the ARCTICS Aurora Field Guide (Herlingshaw et al., 2024).

2. The Skywarden moderating team routinely review each report submission and, as part of this process, assess which auroral forms are present in the submitted ma-

terial. During this step, the moderator updates the auroral form tags according to their knowledge and (extensive) experience in auroral form identification. This means that not only dunes identified by the observer in step 1 were approved or rejected by the moderator, but also that some observations where dunes were not identified by the observer were marked as containing dunes at this step.

3. Two authors of the present article (MG and EB) visually inspected all the Skywarden observation reports marked as containing dune aurora after step 2. In a few cases when either of them had reasonable doubt about the validity of the identification (e.g. suspicion of low-altitude clouds modulating the diffuse aurora, suspicion of wave structures in airglow rather than dune aurora, barely discernable luminosity modulation in the images), the observations in question were discarded.

During the visual inspection in step 3, we determined the time intervals during which the dunes appeared in the pictures, either using the EXIF information contained in the images (if provided) or indications given by the observers in the free-text description of the observation. When no reliable time information could be retrieved but the dunes were clearly visible in at least one image, we retained the event but without giving it a time stamp (necessary to determine its magnetic local time and the associated driving and geomagnetic conditions). In total, we obtained 308 dune aurora observations, which were made during 61 different events by 183 named citizen scientists from Northern Europe, North America, Australia, and New Zealand (4 reports were anonymous).

In addition, we also collected all the aurora observations reported in Skywarden during the same time interval (1 January 2000–31 December 2025), to serve as a baseline when interpreting the seasonal and local time distributions of reported dune aurora events. To extract these data from Skywarden, we also used the API; we did not restrict the search to observations containing at least one picture in this case, nor did we visually inspect all the reports. In total, we obtained 16 479 aurora observation reports from 2269 individual contributors. Out of these, we retained the 9927 observation reports having both a start and end time, which took place on 1560 individual days.

2.2 SuperMAG indices

For this study, we examined geomagnetic activity using two of the SuperMAG indices, calculated from ground-based magnetic measurements at 1 min time resolution by magnetometers from the SuperMAG network (Gjerloev, 2012). We used the SuperMAG Electrojet (SME) index (Newell and Gjerloev, 2011) as a measure of substorm activity, and the SuperMAG Ring current (SMR) index (Newell and Gjerloev, 2012) as a measure of geomagnetic storm activity. We downloaded the SME and SMR indices at 1 min resolution from January 2000 to December 2025.

2.3 OMNI data

We retrieved solar wind and interplanetary magnetic field (IMF) measurements at 1 h time resolution between January 2000 and December 2025 from the OMNI database (Papitashvili and King, 2020). The OMNI data consist of solar wind parameters and IMF observations made by various spacecraft at the L1 Lagrange point of the Sun–Earth system and propagated to the Earth's bow shock, as well as selected geomagnetic indices (King and Papitashvili, 2005). For this study, we considered the following OMNI parameters: solar wind proton number density, speed and dynamic pressure, as well as total IMF magnitude, and its B_y and B_z components in the Geocentric Solar Magnetospheric (GSM) coordinate system.

2.4 IMAGE data and calculation of equivalent ionospheric currents

We use 10 s resolution data from the International Monitor for Auroral Geomagnetic Effects (IMAGE) network to examine ionospheric equivalent currents associated with dune aurora observations. IMAGE currently consists of 57 ground-based magnetometers located in Fennoscandia and surrounding areas. It enables evaluating the ionospheric equivalent currents with a spatial resolution down to about 100 km, hence resolving the so-called mesoscale current structures. One method to derive equivalent currents, known as the Spherical Elementary Current System method (SECS), was introduced in Amm (1997) and has been widely used since then (e.g. Vanhamäki and Juusola, 2020).

3 Results

3.1 Geographic, monthly, and local time distributions of dune events

Figure 2 shows an overview of all the dune observations reported to Skywarden between January 2000 and December 2025. In practice, the earliest observation available at the time of this study was made in 2004, and it is the only one prior to January 2012. The time span of more frequent dune observations still covers approximately one solar cycle. In Fig. 2a–d, the colour of the dots indicates the month when the observation took place.

The dune aurora reports come from three main regions (by decreasing number of observations): Northern Europe, Australia and New Zealand, and North America. These regions have particularly active aurora chaser groups exchanging knowledge and information via social media pages. These groups contribute to Skywarden – but also to other platforms such as Aurorasaurus (MacDonald et al., 2015) – with

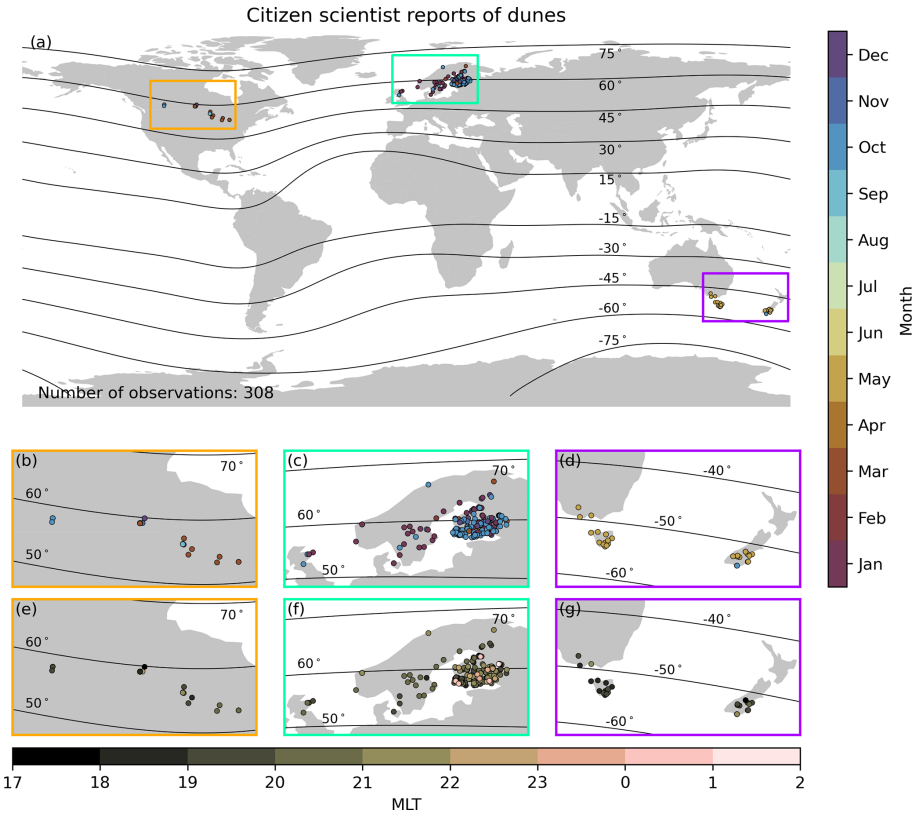

Figure 2. (a) Overview of the reported dune observations around the world. The colour of the dots indicates the month when the corresponding observation took place. Zoom-in with the same colour code over **(b)** North America, **(c)** Northern Europe, and **(d)** Australia and New Zealand. **(e–g)** Zooms-in over the same three regions but with dots coloured according to the MLT of the dune observations. The black lines indicate geomagnetic latitude isocontours, obtained from the AACGM-v2 library (Shepherd, 2014).

their observations. In the North American sector, there are a few observations from Manitoba, Alberta, and Michigan made during the northern-hemisphere autumn, winter, and spring. In the European sector, while the vast majority of reports come from Finland, there is also a number of them from Sweden, and a couple from Norway, Denmark, and Scotland. Most observations were made during the northern-hemisphere autumn and winter, and a few of them in early spring. In New Zealand and Australia, almost all observations were made in May; these correspond to the May 2024 geomagnetic storm. In all three sectors, dune aurora observations were predominantly made near or below 60° geomagnetic latitude, that is, at latitudes usually considered subauroral.

Figure 2e–g show the same observations but with dots coloured according to the magnetic local time (MLT), calculated with the AACGM-v2 Python library (Shepherd, 2014; Burrell et al., 2020). When it is not possible to determine accurately enough the time stamps in a given Skywarden observation (this is the case for 28 observations), the MLT is not calculated, and the corresponding observations are not shown in these figures. When multiple dune images were included in a given observation report, or when the observer provided the time interval during which they photographed dune aurora, we retain the earliest time with a dune image to calculate the MLT. While MLT hours range from 17.5 to 1.2 across individual dune observations, one can see that most observations started in the pre-midnight sector.

In Fig. 3a, we show the MLT distribution of individual dune events. A dune event is defined such that observations that took place on the same night and within the same longitude sector (within 40°) are considered forming part of the same dune event. This results in a total of 61 dune events, for which we determine the earliest and latest MLT associated with dune observations. The histogram shown in Fig. 3a is built in such a way that, for each 1 h bin, we count how many dune events include observations within that bin. For instance, if an event includes an earliest dune observation at an MLT of 18.2 and a latest one at an MLT of 23.5, it will increment the following histogram bins: 18–19, 19–20, 20–21, 21–22, 22–23, and 23–0. It is clear that the large majority of dune events include observations predominantly between 18:00 and 01:00 MLT (89 % of them before magnetic midnight), with a peak within 21:00–22:00 MLT.

In Fig. 3b, we show the monthly distribution of individual dune events. This distribution exhibits a main peak in Octo-

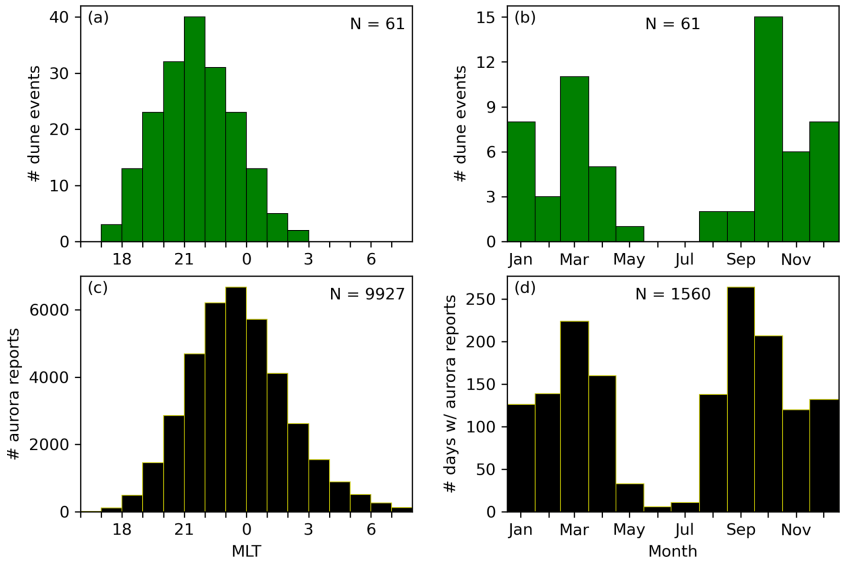

Figure 3. (a) MLT distribution of the dune observations, combining reports from multiple observers during each event. **(b)** Monthly distribution of individual dune aurora events. **(c)** MLT distribution of all aurora observation times. **(d)** Monthly distribution of individual days with aurora observations in Skywarden.

ber (15/61 events, 25 %), a secondary one in March (11/61, 18 %), and contains the majority of the remaining events in the other months of the northern-hemisphere winter and early spring (November to April). There are only a couple of events in May, August, and September, and no events in June and July. This absence of events during the Northern-hemisphere summer months is to a great extent explained by the fact that most Skywarden contributors are based in Northern Europe, where nights are bright during that time. It is only recently (particularly after the May 2024 geomagnetic storm) that Skywarden became known to the Southern-hemisphere aurora chaser communities, which is why there are currently only a few dune events reported from those latitudes that could in principle bridge the gap during those months (southern-hemisphere winter).

Citizen science observations are not continuous and bear some bias related to the typical human behaviour, such as staying awake past sunset, sleeping at night, and waking up around or after sunrise. Aurora chasers are also more likely to go out and collect data when a geomagnetic storm is predicted to occur, and may not stay outside for the entire duration of the auroral displays, which can lead to an over-representation of earlier MLTs in the collected observations. As it is known that the occurrence rate of auroras is not evenly distributed throughout the year, we compare the MLT and monthly distributions of dune events with a baseline given by all the available aurora observations from Skywarden. Figure 3c shows the MLT distribution of the 9927 aurora observation reports having a start and end time retrieved between January 2000 and December 2025, the histogram bins being incremented similarly as for the dune events (see above). While a slight bias can be seen for aurora observations taking place in the earlier half of the night, the overall distribution is nonetheless relatively symmetric and has its peak between 23:00 and 00:00 MLT, i.e. two hours later than that of the dune observations. This suggests that the dunes are predominantly a pre-midnight phenomenon, with an increased likelihood to occur in the few hours after 18:00 MLT. The monthly distribution of all aurora event dates is given in Fig. 3d. Here, for simplicity, we simply retain individual days with at least one aurora report in Skywarden without considering the longitudes, such that, for instance, the 11 May 2024 is counted only once. A similar figure but considering only the Skywarden reports originating from the European sector is given in Appendix C (Fig. C1). We can see that the distributions are largely similar to those given in Fig. 3, the main difference being the number of dune events in March, of which a noticeable fraction originates from outside Europe.

The histogram shown in Fig. 3d reveals two peaks around the equinoxes (March and September). Notably, 74 % of dunes events and 95 % of all aurora events in Skywarden were observed in Finland. This highlights the importance of analysing local observation conditions, such as cloudiness and darkness conditions, when interpreting the monthly distribution of observed events. In Appendix B, Fig. B2 shows the monthly average of cloudiness in Finland, obtained from the Finnish Meteorological Institute past weather database. We consider nighttime cloudiness expressed in okta (a scale quantifying the fraction of the sky covered with clouds, ranging from 0: fully clear, to 8: overcast). Nighttime is defined when the solar elevation at ground level at a given meteorological station is at least 10° below the horizon (i.e. the solar zenith angle is greater than 100°). Across Finland, the

average cloudiness during the darkest winter months (from November to January) typically ranges between 6 and 7 okta, whereas observing conditions are better in spring (March and April) and early autumn (September). This likely explains to a great extent the peaks in auroral observations reported in Skywarden in March and September (Fig. 3), in addition to the Russell–McPherron effect (Russell and McPherron, 1973) which leads to enhanced geomagnetic activity during equinoxes. Besides, as mentioned earlier, the deep trough in dune and auroral observations between May and July is due to the fact that, during that period of the year, nights are not dark enough in Finland for the aurora to be visible. Given that the vast majority of the reports in Skywarden are from Finland, this effect greatly shapes the monthly distributions shown in Fig. 3b and d.

Interestingly, September is a month for which only two dune aurora events have been recorded (Fig. 3b), whereas the largest dune event occurrence peak is in October (15 events, 13 of which are from Europe according to Fig. C1b). The majority of dune events in October were indeed observed in Finland, which has a monthly average nighttime cloudiness close to 6 okta (in comparison, for September it is under 5 okta). These relatively unfavourable observation conditions suggest that it is likely that recorded events contain only a fraction of all dunes events occurring in October. We also note a low number of dune events in February, not reflected in the all-aurora distribution. If not simply due to too small a number of events for the monthly statistics to be robust, the dominance of October and relative lack of dune events in February and September may suggest that the dunes require conditions that are not only related to geomagnetic activity. A possible factor leading to a lower number of dune events in September compared to October is the fact that the early evening hours, when the dunes are typically observed, are not dark in early September. The fact that equinoxes occur around 20 March and 23 September rather than in the middle of those months implies that evening hours are slightly darker in March than in September, hence making it more favourable for the dunes to be observed in March than in September. Nevertheless, this bias in darkness conditions cannot alone explain the low number of dune events in September, as April – when the Sun sets at later hours than in September – has noticeably more (5, all from Europe) dune events than September. Hence, the September–October difference in dune event number might also, for instance, have something to do with atmospheric dynamics which have their own seasonal patterns.

3.2 Dune event duration

Citizen scientist observations of the aurora are not continuous and hence they are unlikely to capture the dune events in their entirety. However, the large database provided by Skywarden observations enables us to determine conservative lower-boundary estimates of dune observation durations, when either multiple photographs are appended to the Skywarden record or the observer indicated in the description text within which time range they have dunes in their images. Out of the 308 Skywarden dune observations used in this study, this is the case for 151 of them.

Figure 4a gives the distribution of dune observation durations as determined from individual Skywarden reports. While approximately a third of them (53/151) were photographed for less than 15 min, the distribution exhibits a gradual decrease with increasing durations, including a non-negligible tail beyond 1 h amounting to about 15 % (23/151) of the observations. Three observations included dune photographs for more than three hours; the first one was reported from Finland on 23 October 2022 (3.2 h), the second one from Tasmania on 11 May 2024 (4.2 h), and the third one from Finland on 12 December 2025 (3.1 h). Multiple factors need to be met for the totality of a dune display to be recorded by a single observer. For instance, the observer needs to be photographing before the dunes appear and until they have vanished, and they need to keep the camera pointed in the direction of the dim dune aurora rather than turn it towards brighter and more dynamical auroral structures. Therefore, we consider the distribution shown in Fig. 4a a lower-boundary estimate of the true duration of the corresponding dune displays. To get a more comprehensive overview of the duration of dune events, we can combine the information contained in multiple observations of the same event. Figure 4b shows the distribution of dune event durations based on multiple (when available) reports by observers. Only dune events for which either several reports were made or a single report containing information on the duration of dune presence in images are shown in the figure. This is the case for 47 out of the 61 dune aurora events considered in this study. We can see that only half of these events (23/47) have a duration less than an hour, ~ 20 % (9/47) of them were photographed for between one and two hours, and about a third of them (15/47) have been recorded for more than two hours. Five events are of particularly long duration: the 7 October 2015 event observed from Finland and Scotland (3.8 h); the 17 December 2023 event observed from Finland (4.1 h); the 13 March 2022 event also observed from Finland (4.8 h); the 20 January 2016 event observed from Finland, Norway, and Scotland (5.2 h); and the 11 May 2024 event observed from New Zealand and Australia (6.9 h). This confirms that dune aurora can cover a wide region and last for multiple hours, as was noted in Grandin et al. (2021).

A version of Fig. 4 for European observations only is provided in Appendix C (Fig. C2). No major differences can be noted between the two figures.

3.3 Distribution of dunes as a function of solar wind and geomagnetic activity

To assess whether dune aurora is associated with specific solar wind driving conditions, we compare the distribution of

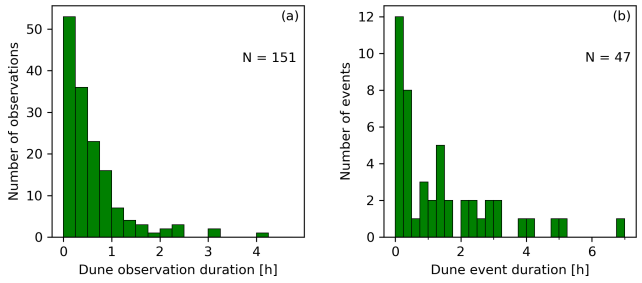

Figure 4. Distributions of the duration of **(a)** dune observations (i.e. by a single observer), and **(b)** dune aurora events (i.e. combining multi-observer observations of the same event). These are conservative lower-boundary estimates based on the information available in the Skywarden observation logs.

selected solar wind and IMF parameters (solar wind proton number density, speed, dynamic pressure, IMF magnitude, and IMF B_y and B_z components in the GSM coordinate system) associated with dune events and associated with all the aurora observations from Skywarden. This is shown in Fig. 5, where histograms corresponding to dune events are given in green whereas those for all aurora observations are in black. The total number of data points is given in the top-right-hand corner of each panel, as are the values of the lower quartile, median, and upper quartile.

For every dune event and Skywarden aurora report, the driving parameters are retrieved from the 1 h OMNI data. We retain the average between the value of each parameter two hours and one hour prior to the start time of the observation (that is, two values), to account for the time delay between the arrival of the measured solar wind and IMF at the Earth's bow shock (as given by OMNI data) and their effects in the magnetotail (e.g. Rong et al., 2015; Pitkänen et al., 2016). For the dune events (green histograms), we consider the driving conditions during the two hours preceding the earliest dune aurora observation (average value during the two-hour window), such that a given event is associated with a single value of the solar wind and IMF parameters.

Figure 5a–f suggest that dune aurora observations do not tend to take place when solar wind driving is significantly different from during typical aurora observations. The only possibly meaningful difference is found in the solar wind density, with a median value for dune aurora events of 8.8 cm^{-3}, compared to 7.2 cm^{-3} for all-aurora observations. As we will see in Sect. 3.4, this difference is however not statistically significant. Regarding the IMF, we note that the total magnitude distributions exhibit a similar situation as the solar wind density, with a slight tendency for dune events to be associated with higher values (median of 9.6 nT) than all-aurora observations (median of 8.6 nT). Differences in IMF B_y and B_z distributions are marginal. Here too, the differences are not statistically significant. For comparison, we made a similar figure considering only the observations from the European sector (Fig. C3 in Appendix C), which shows very similar distributions as those presented in Fig. 5.

Next, we examine the distribution of dune aurora observations with respect to geomagnetic latitude, together with geomagnetic activity as measured with the SME and SMR indices. Figure 6a shows the geomagnetic latitudes of dune observations as a function of time, with red stars corresponding to northern-hemisphere latitudes and blue stars corresponding to southern-hemisphere latitudes. This way of displaying the data enables one to visualise the latitudinal spread of dune observations during individual events. We can see for instance observations spanning more than 5° in geomagnetic latitude during the 7 October 2015 event (57.2–64.0° N), the 7 October 2018 event (55.4–60.4° N), the 14 January 2022 event (54.0–63.9° N), the 17 December 2023 event (57.6–63.7° N), and the 11 May 2024 event (47.9–54.4° S). This suggests that the dunes may be relatively widespread during some events, although one needs to take into account the uncertainty in their exact location (see discussion in Sect. 4). In Fig. 6b, the same data are displayed as a histogram, peaking at latitudes a few degrees below 60°. Considering the data from both hemispheres, 92 % of the dune observations were made at a geomagnetic latitude below 61°. For comparison, the geomagnetic latitude distribution of all aurora observations retrieved from Skywarden is shown in Fig. 6c. While it is difficult to assess whether the fact that this distribution peaks slightly polewards from that of the dune observations is significant, we note that it contains a more prominent tail beyond 60°, and the fraction of reports from below 61° geomagnetic latitude is 74 %. Keeping in mind that these distributions are certainly biased by the over-representation of observations from southern Finland compared to other regions of the world, this is consistent with the hypothesis that dunes may be a phenomenon more often observed in the equatorward part of the auroral oval.

Figures 6d–i present, in a similar format as the above panels, the distribution of the SME and SMR indices during the dune and all-aurora observations. These two indices are measures of substorm and geomagnetic storm activity as they are proxies for auroral electrojet and ring current, respectively. Since SuperMAG indices are provided at 1 min temporal resolution, and given that the aurora observations do not have such a high temporal resolution, we retain a 30 min average of the SME and SMR indices around the start time of each observation (i.e., between 15 min before and 15 min after that time stamp). The main results that can be inferred from these figures are the following:

1. During a dune event, SME and SMR values can change significantly (see Figs. 6d, g). This implies that the dunes span across not only a large geographic zone as discussed above, but also during a significant time interval. This is consistent with the findings from Fig. 4 that dune events can last for up to several hours, a time over which SME and SMR can vary significantly.

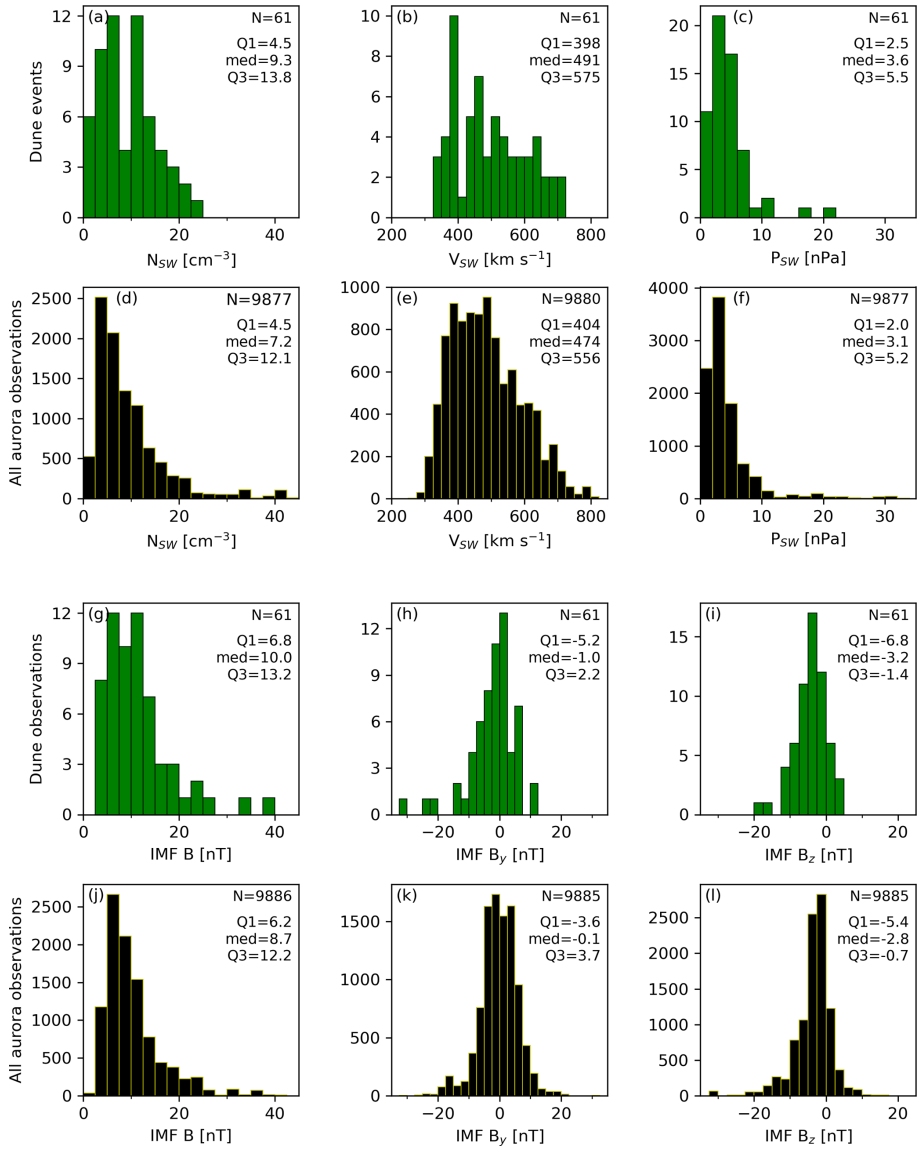

Figure 5. Solar wind and IMF parameters associated with dune events (green histograms) and all aurora observations (black histograms). The considered parameters are: **(a, d)** solar wind proton number density; **(b, e)** solar wind speed; **(c, f)** solar wind dynamic pressure; **(g, j)** IMF magnitude; **(h, k)** IMF B_y component; and **(i, l)** IMF B_z component.

2. Generally, the dunes are seen when auroral electrojet intensity is elevated (50 % of the observations were made with SME within 649–1143,nT; see Fig. 6e). It however does not need to be extreme, as the median value of SME is 871 nT, but it is significantly higher than the median value of SME for all aurora observations (507 nT, Fig. 6f).

3. Likewise, the dunes tend to be observed when geomagnetic activity is enhanced (median SMR value: −49 nT; see Fig. 6h), though they do not require a strong geomagnetic storm for which a threshold of −100 nT is generally retained (e.g. Gonzalez et al., 1994; Zhang et al., 2008; Nitta et al., 2021). We note however that, if the dunes do appear during a geomagnetic storm, this analysis does not assess whether the threshold of −100 nT is attained at any point during the storm, before or after the dune observations. Still, the distribution of SMR index values associated with dune observations is skewed towards more strongly negative values than that obtained by considering all aurora observations (Fig. 6i). This could be partly related to the fact that the dunes are often seen away from the magnetic midnight sector, hence stronger geomagnetic storm activity is needed to bring the optical emissions to the relevant latitudes compared to typical aurora.

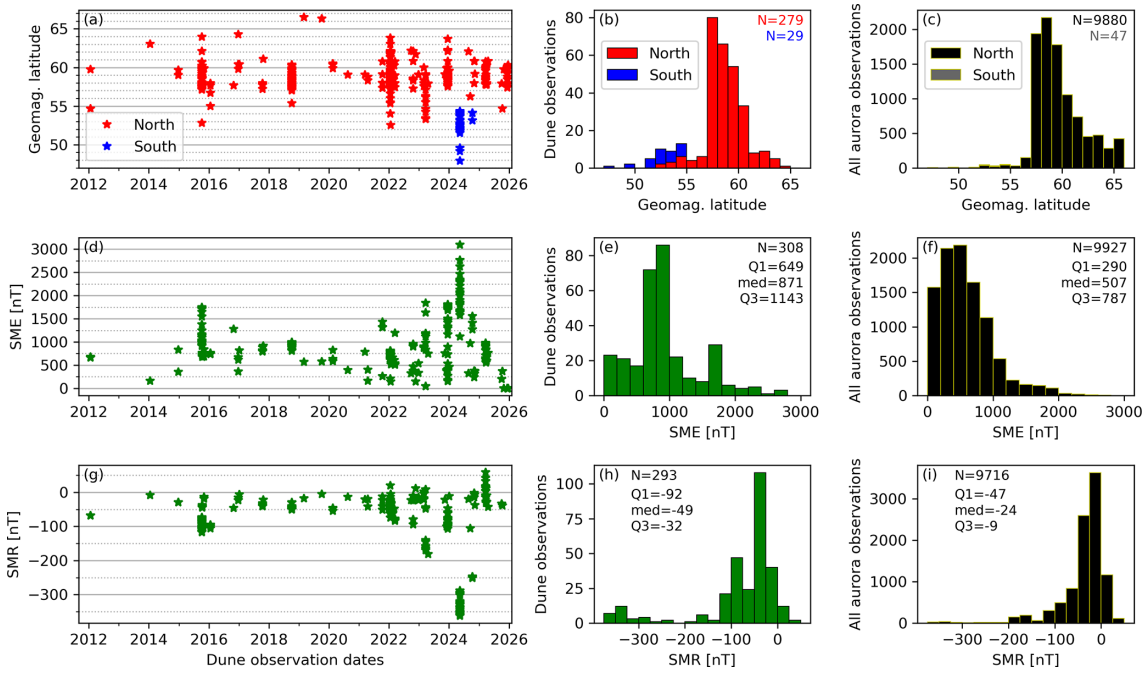

Figure 6. (a) Geomagnetic latitude of dune observations (individual reports) as a function of the observation dates, and **(b)** corresponding distribution. Northern-hemisphere latitudes are shown in red and southern-hemisphere latitudes (projected to the northern hemisphere) in blue. **(c)** Geomagnetic latitude distribution of all aurora observations; northern-hemisphere latitudes are shown in black and southern-hemisphere latitudes in grey. **(d)** SME index of dune observations as a function of the observation dates, and **(e)** corresponding distribution. **(f)** SME index distribution of all aurora observations. **(g–i)** Same for the SMR index.

A similar figure considering only Skywarden reports from the European sector is given in Appendix C (Fig. C4). We can see that, while the distributions overall resemble well those shown in Fig. 6, the strong-activity (in terms of SME and SMR) tails are absent: there are no dune observations associated with SME > 1800 nT nor with SMR < -200 nT. A likely explanation is that the North American and Oceanian dune observations, mainly originating from lower geomagnetic latitudes than the majority of those from the European sector (see Fig. 2), require higher geomagnetic activity to bring the auroral oval within the field-of-view of the observers. This is a further indication that the dunes can appear under various levels of geomagnetic activity, from moderately enhanced to fairly extreme.

3.4 Statistical significance of deviations of dune aurora distributions from all-aurora distributions

We evaluate the statistical significance of the differences between the distributions of dune events and the distributions of all aurora observations from Skywarden by carrying out permutation tests. For each considered parameter (MLT, monthly occurrence, solar wind density, solar wind speed, solar wind pressure, IMF magnitude, IMF B_y and B_z components, and SME and SMR indices), we assess whether the differences in key properties of the dune histograms (green) and all-aurora histograms (black) can be explained by chance, if sampling a small number of reports (61, i.e. the number of dune events) out of all the Skywarden reports of aurora observations.

We perform each permutation test with 20 000 iterations based on the histograms shown in Figs. 3, 5, and 6 as follows:

1. We quantify the difference ("effect size") between dune and all-aurora distributions according to a selected statistic (circular mean for MLT, total variation (TV) distance for monthly distribution, median for all the other parameters). Given two histograms P and Q, TV is defined as $\frac{1}{2}\sum_i |P_i - Q_i|$; it varies from 0 (fully identical distributions) to 1 (fully disjoint distributions), with intermediate values giving the fraction of total variation.

2. We carry out 20 000 iterations of random sampling (without replacement) of the reference (all-aurora) distribution with the number of dune aurora events (61), and assess how frequently the random sampling leads to a difference (with respect to the reference distribution) larger than the one between dune and all-aurora distributions. We express this result as the p-value of the permutation test.

3. We assess the significance of the effect after false discovery rate (FDR) correction to a significance level of 0.05 (Benjamini and Hochberg, 1995). This is achieved by computing the q-value of the test (Storey, 2002).

The results of this analysis are summarised in Table 1. We can see that the difference in the circular mean of the MLT of dune aurora events compared to all aurora observations is highly significant in the statistical sense, as are the differences in the median values of the SME and SMR indices. Although to a lesser extent, this analysis suggests that the monthly distribution of dune aurora events differs significantly (by 28 % in total variation) from that of all aurora observation reports from Skywarden. However, none of the solar wind and IMF parameters passes the significance test. This indicates that it is unlikely that dune aurora events are associated with a set of driving solar wind and IMF conditions that stand out from those associated with the whole range of auroral observations reported in Skywarden. A similar analysis of statistical significance of differences in distributions for dune aurora compared to all aurora observations, but restricted to observations from the European sector, is presented in Appendix C (Table C1). The conclusions are the same.

One should in addition keep in mind that this analysis assesses the statistical significance of the differences between dune aurora events and all-aurora observations as reported in Skywarden, which are themselves affected by biases at various levels. Those results should therefore not be interpreted as strictly depicting the statistical occurrence rates and properties of dune aurora intrinsically, but rather in terms of observations thereof as reported in Skywarden. Inferring the intrinsic statistical properties of dune aurora would require being able to accurately model the observational effort, which is affected by citizen scientist behaviour, weather conditions, social media dynamics, equipment sensitivity and settings, among other parameters. Quantifying this observational effort and normalising the dune parameter distributions accordingly would prove an extremely complex task that lies beyond the scope of this study.

3.5 Equivalent currents associated with dune aurora

In the study of the first dune event by Palmroth et al. (2020), it was noted that the dunes occurred in concert with a strong eastward electrojet. Here, we leverage the larger dune event database provided by Skywarden reports to assess whether this is a typical situation for all dune events.

We first identify the dune events for which at least three clear dune observations have been made in the same geographic area, such that we have an indication of a nonzero time period over which the dunes were photographed. We only retain dune observations from the Fennoscandian sector, where ground-based magnetometers from the IMAGE network are close enough to each other to resolve mesoscale patterns (that is, ~ 100 km horizontal scales) in equivalent currents. When, for a given dune event, the observations span more than 6° in geographic longitude (~ 330 km in the east–west direction for geographic latitudes around 60°), the observations are separated into subgroups according to their geographic longitude (in longitude bins of equal width). In three cases, the observations are split into two subgroups, and in one case (spanning 15.9° in geographic longitude) they are split into three subgroups. We obtain 15 sets of observations (corresponding to 10 individual dune events) for which the equivalent current analysis can be carried out.

Table 2 summarises the results of the equivalent current analysis. The first column gives the date and time interval within which the dunes were photographed during the retained observations. The second column indicates the number of observations, for which the mean geographic coordinates of observers are given in the third column. The fourth and fifth columns indicate whether the dunes were observed in conjunction with the eastward (E) or westward (W) electrojet and with the Harang discontinuity, respectively. This was assessed by visual inspection of the equivalent current figures, some examples of which are given in Figs. 7–9.

In practice, for each set of observations, the SECS analysis method is carried out using all the available IMAGE stations. The results are presented in the form of keograms of the geographic east (ϕ) and south (θ) components of the yielded equivalent current density ($\boldsymbol{J}_{\mathrm{eq}}$) as a function of time and geographic latitude, for the mean longitude of the dune observations, as exemplified in Fig. 7a–b for the 12 December 2025 event observations from the Finnish sector. Additionally, equivalent current maps can be displayed (see Fig. 7c), wherein horizontal current direction and magnitude are indicated with black arrows and the curl of the equivalent currents, which is a proxy for field-aligned current density (e.g., Weygand and Wing, 2016), is shown as the background colour. In the following, we look in more detail at such results for three selected events exemplifying the various configurations with respect to the eastward and westward electrojets.

It appears from Table 2 that there are three types of situations when it comes to the coincidence of the dune aurora with the auroral electrojets. In 10 cases, the dunes are found to occur within the eastward electrojet, like in Palmroth et al. (2020). However, in one case, they are taking place within the westward electrojet, and in the remaining four cases they start within the eastward electrojet but remain visible throughout the transition to the westward electrojet. Besides, all events appear to take place in the vicinity of the Harang discontinuity.

Figure 7 shows an example of a set of dune observations associated with the eastward electrojet and a clear Harang discontinuity. In Fig. 7a and b, the keograms have been obtained along the meridian whose longitude corresponds to the average of the observers' longitudes. Note that the horizontal line appearing around 68° latitude in Fig. 7b is an artifact produced by the analysis, which does not affect the region we are interested in here. The mean geographic latitude of observers' locations is indicated with a horizontal dashed line, and the two vertical dashed lines mark the earliest and the latest dune photograph from that set of observations, respectively. Throughout the time interval during which dunes have

Table 1. Evaluation of the statistical significance of the differences between the dune and all-aurora distributions shown in Figs. 3, 5, and 6. Differences are assessed using permutation tests (20 000 iterations) with false discovery rate (FDR) correction. Depending on the considered parameter, the statistics used are either circular mean (for MLT), TV distance (for monthly distribution), or median (for solar wind parameters, IMF, and geomagnetic indices).

Parameter	Effect size (statistic)	p-value	q-value	Significant (FDR 0.05)
MLT	2.1 h (circular mean)	$< 5 \times 10^{-5}$	0.00017	Yes
Monthly occurrence	0.28 (TV)	0.00140	0.00350	Yes
SW density	2.1 cm^{-3} (median)	0.03260	0.06520	No
SW speed	17 $km\,s^{-1}$ (median)	0.33988	0.42485	No
SW pressure	0.52 nPa (median)	0.09805	0.14006	No
IMF $\lvert B \rvert$	1.4 nT (median)	0.07225	0.12041	No
IMF B_y	0.90 nT (median)	0.41203	0.43873	No
IMF B_z	0.45 nT (median)	0.43873	0.43873	No
SME	364 nT (median)	$< 5 \times 10^{-5}$	0.00017	Yes
SMR	24.5 nT (median)	$< 5 \times 10^{-5}$	0.00017	Yes

Table 2. Equivalent current analysis of dune aurora events having several observations. For each event, we indicate the number of observations retained and their mean geographic coordinates. We examine whether the dunes are associated with the eastward (E) or westward (W) electrojet (an arrow indicates a transition from one to the other) and if they take place near the Harang discontinuity. The events shown in Figs. 7–9 are marked with *.

Event date and time (UTC)	Number of observations	Mean coordinates of observations (geogr.)	Associated electrojet	Harang discontinuity
2015-10-07 16:58–18:43	16	61.2° N, 22.8° E	E → W	Present
2015-10-07 16:51–18:37	12	62.5° N, 28.2° E	E → W	Present
2015-10-12 18:09–18:34	5	61.5° N, 22.9° E	E	Present
2017-10-13 16:30–17:53	3	60.8° N, 24.6° E	E	Present
2018-10-07 17:27–18:04	17	61.3° N, 23.4° E	E	Present
2018-10-07 17:15–18:05	15	61.7° N, 26.5° E	E	Present
2022-01-14 19:00–21:32*	8	60.1° N, 14.5° E	E → W	Present
2022-01-14 19:09–20:07	4	61.8° N, 19.3° E	E	Present
2022-01-14 18:33–20:41	34	62.4° N, 25.8° E	E	Present
2022-10-23 16:31–19:45	3	63.3° N, 27.5° E	E → W	Present
2023-02-26 20:45–21:07*	4	61.4° N, 24.9° E	W	Present
2023-12-17 15:29–17:35	8	61.2° N, 23.0° E	E	Present
2023-12-17 15:34–16:53	14	62.5° N, 26.2° E	E	Present
2025-03-21 19:15–20:21	7	62.2° N, 28.0° E	E	Present
2025-12-12 17:45–20:50*	12	61.7° N, 26.8° E	E	Present

been photographed from Finland, the observers are close to the equatorward edge of the eastward electrojet. It is important to note that the dunes may have been present before the earliest reported observation and after the latest one, and that it is also possible that the dunes were not necessarily visible at all times during the marked time interval.

Figure 7c shows the equivalent current map at a time approximately halfway through the set of observations. The large-scale features of the reconstructed equivalent currents clearly exhibit a well-delimited and relatively strong (scale shown in the top-left corner of the panel) eastward electrojet between the region-1 (upward, in red) and region-2 (downward, in blue) field-aligned currents. Near the eastern edge of the resolved area, the reversal in the horizontal current direction with increasing latitude indicates the presence of the Harang discontinuity. The individual observers' locations are shown with white stars. To provide a measure of the uncertainty in the actual location of the dunes, we have added a circle around each star, with a radius of 463 km corresponding to 10° elevation at 100 km altitude (see also this point in the Discussion, Sect. 4). We can see that, despite the uncertainty in the exact dune aurora location, for all observations they are unambiguously located within the eastward electrojet. The yellow star indicates the mean location of the observers, which is used for making the keograms in the other two panels of the figure.

In a few cases, the dune observations start within the eastward electrojet but continue after transitioning to the west-

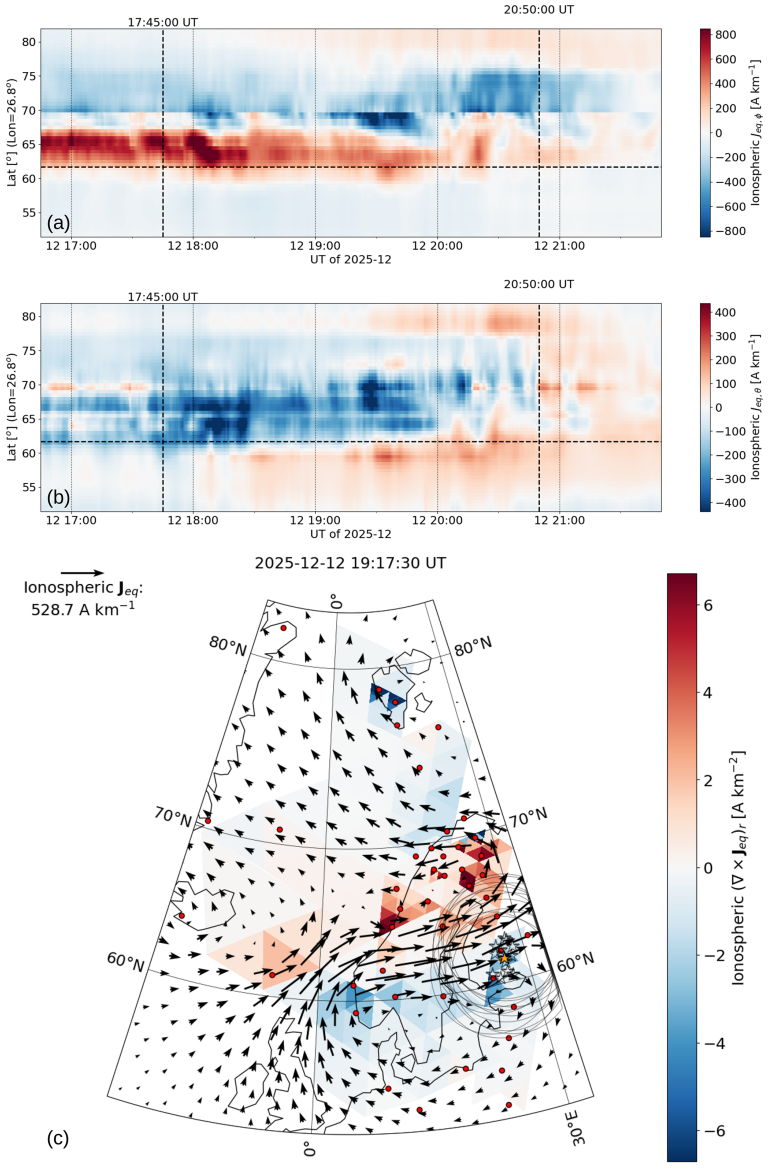

Figure 7. Equivalent current analysis applied to dune observations in the Finnish sector during the 12 December 2025 event. **(a)** ϕ (positive eastwards) component of the equivalent currents. The horizontal dashed line indicates the average geographic latitude of the dune observations; the vertical dashed lines indicate the earliest and latest dune observations. **(b)** θ (positive southwards) component of the equivalent currents. **(c)** Map of the equivalent currents at 19:17:30 UT. The colour scale indicates the curl of the calculated equivalent currents, with positive (negative) values being a proxy for upward (downward) field-aligned currents. The arrows indicate the direction and magnitude (scale given in the top-left corner of the panel) of the horizontal currents. The locations of the dune observers during this event are indicated with white stars; they are surrounded with circles representing the uncertainty in the actual location of the dunes (see text). The yellow star shows the mean location of the retained dune observations, and magnetometer stations used in the SECS analysis are shown with red dots.

ward electrojet. An example of such events is given in Fig. 8 with the observations of the 14 January 2022 event within the Swedish sector. The eastward component of the equivalent currents near the observers' mean location (Fig. 8a) is positive until ∼ 20:40 UT, after which it is negative, corresponding to a westward current. We note that the last reported observation of dunes in the sector (at 21:32 UT, vertical dashed line) seems to match the disappearance of a patch of eastward current at high latitudes (above 65°). This might however be a mere coincidence. Figure 8c shows the equivalent current map at 20:16 UT. A clear Harang discontinuity signature can be seen to the north-east from the observers' locations.

Finally, an example of dune observations reported in conjunction with the westward electrojet is given in Fig. 9. Four observers from Finland shared photographs of the event, which took place on 26 February 2023 and had observa-

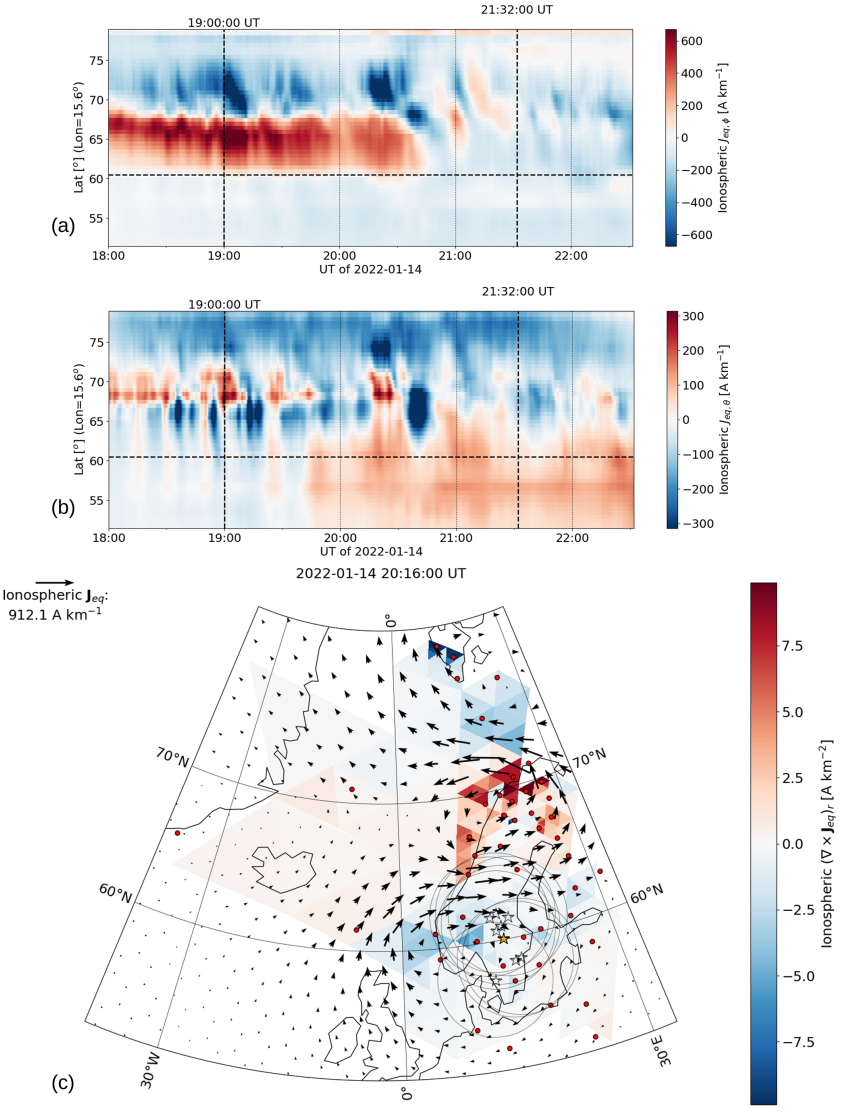

Figure 8. Equivalent current analysis applied to dune observations in the Swedish sector during the 14 January 2022 event. Same format as Fig. 7.

tions only during a relatively brief time interval (22 min). The SECS analysis unambiguously indicates that, at the time of those observations, the Finnish sector was within the westward electrojet (Fig. 9a and c). However, it cannot be excluded that the dunes were present at an earlier time but were simply not observed.

These three examples reveal that, while dune aurora seems to favour eastward electrojet conditions to appear, it can also be seen within the westward electrojet. It is important to stress that, as the dunes are generally accompanied by brighter auroral displays, the spatio-temporal patterns in the electrojet currents likely reflect the dynamical changes in the active auroral structures rather than those of the dunes themselves.

4 Discussion

Before discussing the results obtained from this study in light of the existing literature, we should mention a few caveats related to the nature of our main dataset. First of all, while all the Skywarden observations used in this study have been visually inspected to validate the presence of dunes in at least one image (see details in Sect. 2.1), we cannot be entirely certain that the time stamps associated with each observations are accurate. However, practices are gradually being harmonised and the quality of the citizen science data is improving fast, thanks to at least three aspects. First, the administrators of social media groups dedicated to aurora chasing play a crucial role by sharing a wealth of knowledge and expertise on how to best document an aurora night. Second, the

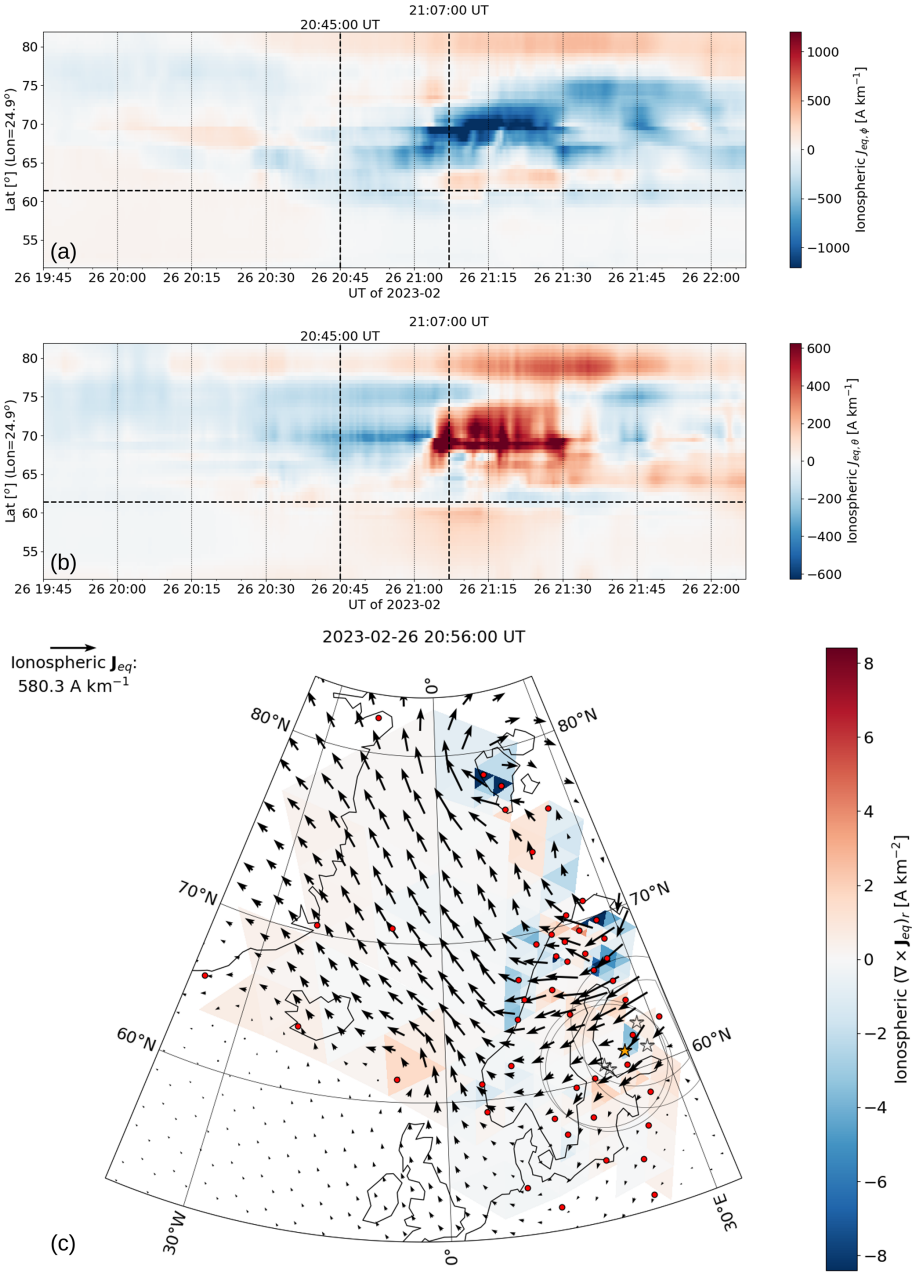

Figure 9. Equivalent current analysis applied to dune observations in the Finnish sector during the 26 February 2023 event. Same format as Fig. 7.

Skywarden moderators inspect the submitted reports and correct mistakes they identify. Third, citizen science data quality has been benefitting from initiatives aiming at coordinating citizen science efforts in auroral science around the world, such as the ARCTICS Aurora Field Guide and Handbook for Citizen Science (Herlingshaw et al., 2024) or the Aurorasaurus project (e.g. MacDonald et al., 2015; Kosar et al., 2018). The main limitations and mitigations we can identify with the used dune observation dataset are the following:

1. The time stamps associated with dune aurora observations may contain errors. In a few cases, it was possible to identify a one-hour offset between the logged observation time and the image time stamps, most probably due to the camera being kept in daylight saving time in winter or vice-versa. These offsets were corrected. For a handful of observations, the time had been indicated in the 12 h format whereas the Skywarden submission form assumes a 24 h format. Such cases were also easily identified and corrected. However, when some

time stamps were too unclear, the corresponding observations were ignored in the part of the analysis highly sensitive to timing (i.e. calculation of MLT of the observations, determination of associated driving parameters and geomagnetic indices, and estimation of the duration of the dune events). This only concerned 28 reports out of 308.

2. Given that the dunes are difficult to image (they are low-contrast structures in the dim diffuse aurora), they are often overlooked, and hence they are likely underreported. Often, when they have been identified by an observer who shares the information with their aurora chasing community, additional reports are submitted to Skywarden as photographers specifically search for dune signatures in their own images.

3. Skywarden being originally and still primarily a Finnish observation system, reports from Central and Southern Finland largely dominate the database. This induces a geographic bias which can be seen in e.g. the geomagnetic latitude distribution and in the monthly distribution of dune observations. Such a geographic bias may also be reflected in the distribution of driving conditions associated with the dunes, as the auroral oval needs to expand enough to be visible from Central and Southern Finland. However, an increasing number of reports have been submitted to Skywarden from other parts of the world, as the system is becoming more widely known.

4. One must also keep in mind that the geomagnetic latitudes associated with dune observations are in fact those of the observer as they were photographing the aurora. The latitude of the dunes themselves may therefore differ by a few degrees, depending on the elevation at which the dunes were located when seen from the observer's location. A conservative estimate of the incurred error in geomagnetic latitude is that the true latitude of the dunes is within $\pm 4.2°$ of the observer's latitude, assuming that they are at an elevation of at least 10° above the observer's horizon and that they lie at approximately 100 km altitude (Palmroth et al., 2020). This corresponds to a distance between the observer's location and the dunes within 463 km, which translates to an uncertainty in terms of longitude of the order of $\pm 8.3°$ for an observer near 60° geographic latitude (corresponding to ~ 0.55 h in MLT). Given that in most observations where dunes are visible the camera pointing is not aligned with the meridional (north–south) direction and the elevation of the dunes is higher than 10°, the geographic (and hence geomagnetic) coordinate and MLT offsets are likely within a narrower confidence interval. Nevertheless, it is important to keep in mind that our results show the distributions of properties associated with dune aurora observations, which are affected by various sources of biases and uncertainties, as discussed above.

Bearing these limitations in mind, it is clear that the dunes have been seen in multiple regions located predominantly near the equatorward edge of the auroral zone, in both hemispheres. While their occurrence pattern is to a great extent consistent with that of aurora observations in general, it exhibits a few peculiarities that may help uncover the formation mechanism of dune aurora.

We first note that the monthly distribution of observed dune events exhibit differences from that of Skywarden aurora reports. Specifically, the month with the largest number of dune aurora events is October, and the months of February and September have notably few dune events given the occurrence rate of the auroral observations reported by the citizen scientists. While it is possible that those anomalies bear large statistical uncertainties due to the somewhat limited number of dune events (61), this may highlight a possible need for specific conditions for the dunes to form, other than geomagnetic activity.

In a study of mesospheric bores at middle and low latitudes between 2013 and 2017 with airglow observations from the Suomi-NPP satellite, Su et al. (2018) found two peaks in their monthly distribution: March through May and October. At high latitudes (Tromsø, 69.6° N), Chauhan et al. (2024) used a ground-based airglow imager to study mesospheric frontal structures including bores between 2011 and 2015. Out of the 18 events they identified, the majority took place in December and January. One important note is that, in that study, only clear-sky nights without auroral activity were considered. The exclusion of nights with auroral activity may have led to a bias favouring the deep-winter months over the equinox periods which are typically more geomagnetically active (Russell and McPherron, 1973). Another extensive statistical study of mesospheric bores was carried out by Hozumi et al. (2019), who observed airglow with the Visible and near-Infrared Spectral Imager on board the International Space Station between September 2012 and August 2015. They looked at the distributions of 306 mesospheric bores as a function of month and local time and found that midlatitude (up to 55° geographic latitude) bores are more frequent during the winter months. Their interpretation is that mesospheric bore formation in this case is likely associated with mesospheric inversion layers produced by migrating tides with large temperature amplitudes at mesospheric heights. The comparison of our dune event monthly distribution with the results from those past studies suggests that, while some aspects are in agreement (e.g. a peak in mesospheric bore occurrence in October), the dunes likely form as the result of a complex combination of processes involving both geomagnetic activity and middle-atmospheric dynamics.

In fact, while the emphasis in previous dune aurora studies has been placed on the mesospheric bore as a candi-

date atmospheric wave playing a role in the formation of dunes (Palmroth et al., 2020; Grandin et al., 2021), other types of waves modulating the neutral density (and hence the density of atomic oxygen, responsible for the green emissions) near 100 km altitude could also be envisaged. In a master's thesis, Seltveit (2022) investigated three dune aurora events observed by airglow imagers in Antarctica and on Svalbard. The analysis of their properties (distance between wavefronts and propagating speed) revealed that, in those cases, the dunes were much more likely to be associated with gravity waves than with mesospheric bores. Their cases, however, generally showed shorter duration compared to the 2016 dune event analysed in Grandin et al. (2021). The shorter durations in those cases suggest gravity wave activity, whereas the longer-lived 2016 event initially appeared more consistent with a mesospheric bore interpretation. Our new survey of observations indicates that the dune event durations can range from much less than an hour to multiple hours. This could suggest that in some cases (typically, shorter event durations) the dunes might be associated with gravity waves, whereas in other cases (typically, longer event durations) they might be associated with mesospheric bores. Meanwhile, climatological results for high latitudes in Antarctica showed that high-frequency gravity waves (periods shorter than 3 h) have minimal variance at the mesopause around equinoxes, implying reduced overall gravity wave activity due to weak filtering winds below 80 km (Beldon and Mitchell, 2010). In the northern hemisphere, a similar trend has been found, with high-frequency gravity wave activity being generally higher during the winter months and reduced in March and September (de Wit et al., 2015). Such gravity waves can have multiple origins in the troposphere, and can also be filtered in association with the polar vortex (e.g. Fritts and Alexander, 2003), and past studies have investigated their capability to propagate upwards and reach the mesosphere and lower thermosphere in relation to the polar vortex. It is well established that this creates a stronger meridional wind towards the winter pole due to stronger gravity wave filtering (Garcia and Solomon, 1985). Besides, according to Kumar et al. (2025), statistically the mesosphere–lower-thermosphere–ionosphere (MLTI) zonal-mean zonal wind responds to the strength of the stratospheric polar vortex. A rapid strengthening of the polar vortex in October could lead to a mean state of weakening of the zonal-mean zonal wind in the MLTI. It is possible that these rapid changes may create unique dynamical conditions in the middle atmosphere that could favour the formation of the dune aurora.

These dynamical background conditions, combined with the monthly patterns in auroral occurrence, darkness hours, and cloudiness, could contribute to explain the monthly distribution of dune aurora reports. Investigating those aspects in more detail could be a natural future avenue for dune aurora research, relying on an interdisciplinary approach (atmospheric sciences and space physics).

The analysis of the distribution of driving parameters associated with dune aurora events has evidenced that the dunes are observed under solar wind driving conditions with no statistically significant difference compared to that of all aurora observations reported in Skywarden. On the other hand, the MLT distribution of dune aurora observations has its peak approximately 2 h earlier than that of all aurora observations from Skywarden, and this difference is statistically significant. This, together with the preference for dunes to occur within the eastward electrojet (with a few exceptions, as presented in Sect. 3.5), suggests that specific evening-sector conditions can favour their formation. As was already hypothesised in Grandin et al. (2021), it is possible that the precipitating particles leading to the diffuse aurora in which the dunes emerge are auroral protons. Ono et al. (1987) showed that when protons precipitate into the upper atmosphere, they produce secondary electrons which can in turn excite the atmospheric constituents, leading to diffuse green emission. This process typically occurs in the equatorward side of the auroral oval and mainly in the dusk sector, which corresponds very well with the location where dunes have been observed – at least when in connection to the eastward electrojet. More recently, Nishimura et al. (2022) found that secondary electrons resulting from proton precipitation could produce a mix of red and green diffuse auroral emissions in the pre-midnight subauroral zone, again consistent with where dunes are most commonly reported. Yet, to be fully conclusive, detailed analyses of individual events with, for instance, satellite observations of precipitating particle fluxes or ground-based spectrometer measurements, are needed.

5 Conclusions

Using citizen scientist observations from the Skywarden database, we have carried out the first systematic survey of dune aurora events. Since 2000, a total of 308 dune aurora observations have been reported into Skywarden, corresponding to 61 individual events which were seen from Northern Europe, North America, Australia, and New Zealand. We have analysed the statistical distribution of dune events as a function of magnetic local time, geomagnetic latitude, driving conditions, and geomagnetic activity. For 15 subsets of dune aurora observations made by several photographers in Fennoscandia (corresponding to 10 individual events), we have applied the SECS method to derive the equivalent ionospheric currents associated with each set of observations.

The conclusions of our study are as follows:

1. The dunes can be observed in various regions of the world, predominantly in the equatorward part of the auroral oval, at latitudes generally located within the subauroral region. This was already suggested in Grandin et al. (2024) but relied on self-reported observations without image-based verification.

2. A given dune event can be observed across a broad region (spanning up to almost 10° in geomagnetic latitude) and last for several hours (up to 6.9 h), indicating that the event studied in Grandin et al. (2021) is not unique in that respect.

3. There does not seem to be any specific type of solar wind driver to produce dunes, as the distributions of solar wind proton number density, solar wind speed, solar wind pressure, IMF magnitude and B_y and B_z components do not exhibit any statistically significant differences for dune events compared to all-aurora observations reported in Skywarden. The dunes are seen throughout the various phases of the solar cycle. They tend to be observed in relation to more enhanced geomagnetic activity compared to that associated with all aurora observations, both in terms of geomagnetic storm activity (SMR index) and auroral electrojet intensity (SME index). This difference is found to be statistically significant.

4. The monthly distribution of dune events is consistent with that of auroral observations, but with a notable difference in the northern-hemisphere autumn equinox (all-aurora event peak in September but dune aurora event peak in October). This difference, which is found to be statistically significant, may partly be explained by a lack of darkness in the early evening hours in September, but may also be related to the monthly distribution of atmospheric waves near the mesopause, or to some other cause yet to be determined.

5. The MLT distribution of dune observations peaks approximately two hours earlier than for all aurora observations (statistically significant difference), suggesting that the dunes might be associated with duskside processes. This could hint at a possible role of precipitating protons.

6. Dune aurora is associated with strong auroral electrojet signatures in ground-based magnetometer data. In most cases, the dunes are colocated with the eastward electrojet, but at least one event was observed within the westward electrojet. In all the analysed events, the Harang discontinuity is present in the immediate vicinity of the dunes. This could indicate a possible role of the nightside transition region in the dune aurora's formation mechanism, requiring further investigation.

Future work will aim at investigating in more detail the possible role of precipitating protons by analysing dune aurora events where supporting satellite and optical ground-based observations are available, and at comparing the yearly distribution of dune observations with that of middle-atmospheric properties to determine what role atmospheric dynamics might play in the formation of dune aurora.

Appendix A: List of the observers whose dune aurora observations reported in Skywarden were used in this study

Aki Karjalainen, Allison Mills, Andrew Clark, Ann-Marie Norlen, Anna Jansson, Anssi Mäntylä, Antero Ohranen, Antti Rinne, Arto Oksanen, Atacan Ergin, Berit Olsson, Bob King, Catharina Nilsson, Christina Sharp, Colin Legg, Cristina Casplin, Cristofer Eriksson, Danny Reardon, Donna Lach, Eero Karvinen, Eila Tiirinen, Elenore Olsson, Elizabeth Miller, Elizabeth Palmer, Ellis Judson, Emma Bruus, Erik Nyberg, Erkki Rauhala, Esa Pekka Isomursu, Fran Davis, Geir T. Birkeland Øye, Geoff Purchase, Graeme Whipps, Hanna Nilsson, Heidi Rikala, Heikki Jokiranta, Heikki Rantala, Heini Kulmala, Helen L. Chick, Ian Griffin, Iweta Seppälä, Jacqueline Guilford, Jan van den Brom, Jani Laasanen, Jani Lappalainen, Jani Lauanne, Janne Laukkanen, Jari Rajala, Jari Virtanen, Jari Ylioja, Jarkko Alatalo, Jarmo Leskinen, Jennifer Mainka, Jess Burrows, Jesse Kyytinen, Jessica Miller, Jim Perdue, Joanna Herranen, Johan Lundström, Johanna Amnelin, John Andersen, Jorma Mäntylä, Jouni Lehtola, Jouni Raunio, Jouni Riihelä, Ju-Kai Tsai, Juhani Hokkanen, Jukka Hilska, Jukka Kytömäki, Jukka Könönen, Jussi Muukka, Kaj Höglund, Kari Haila, Kari Rytilahti, Kari Saari, Kata Sivunen, Kathy Goltz, Katja Söderström, Kerry Saward, Kimmo Kantola, Kirsi Nikkola, Kjetil Vinorum, Kris Kidd, Kristina Saunders, Lasse Tyrväinen, Leena Aijasaho, Leo Jussila, Les Ladbrook, Lone Athanasakis, Lynette Mackenzie, Malin Englund, Mari Jääskeläinen, Maria Rönni, Markku Heikkinen, Markku Lintinen, Markku Ruonala, Markku Siljama, Markku Sirén, Marko Haapala, Marko Vallius, Marko Vesapuisto, Markus Hotakainen, Matias Takala, Matthew Bissett, Matti Helin, Matti T. Salo, Mauri Korpi, Megan Thomas, Michael Estwik, Michele Aucello, Michele Sadauskas, Mika Yrjölä, Mikael Johansson, Mikko Ankelo, Mikko Peussa, Mikko Silvola, Minna Glad, Minna Koivisto, Minna Lehtimäki, Minna Wires, Nick Keizerwaard, Olli Mantikka, Olli Reijonen, Pasi Tuomainen, Paula Häyrinen, Pauli Sorsakari, Pentti Arpalahti, Perttu Nihtila, Peter von Bagh, Petri Kuossari, Petri Martikainen, Petri Sallinen, Pia Simonen, Pirjo Koski, Raija Kokkola, Rami Valonen, Richard Dunstan, Risto Ennevaara, Rita Baker, Roope Luukkainen, Sakari Ekko, Sami Vähätalo, Samuli Ikäheimo, Santtu Pennanen, Sari Hukka, Sari Pietikäinen, Satu Juvonen, Satu Rajamäki, Shellie Evans, Simon Brandt, Sirpa Pursiainen-Hautala, Stella Rodriguez, Susanne Olsson, Tapio Nylund, Tapio Terenius, Teppo Laitinen, Terhi Törmälä, Tero Sipinen, Therese Forsberg, Timo Alanko, Timo Kantola, Timo Oksanen, Toby Schrapel, Tom Eklund, Tomi Katajamäki, Tommy Lågland, Toni Veikkolainen, Tuija Liunala, Tyler Benson, Ulf Jonsson, Ulla Vornanen, Ulrika Ivergård, Veikko Mäkelä, Vesa Puistovaara, Vesa Särkelä, Vesa Toropainen, Vesa Vauhkonen, Ville Bröijer, Ville Puoskari, Virpi Kauko, Yu Ahu; as well as four anonymous observers.

Appendix B: Cloudiness statistics in Finland

Cloudiness can vary significantly on relatively short spatio-temporal scales. Depending on the cloud altitude, even physically small clouds can cover a large portion of the field of view valued by the aurora observer. Matching the interference due to cloud coverage with ground-based aurora observation count exactly would be a challenging task, especially in a citizen science survey. The need for precise location, extent, altitude and observing times of the cloud coverage, matching set for the aurora observations as well as precise position of the aurora despite the cloudiness at the observers location makes it very complex and could warrant a dedicated study of its own.

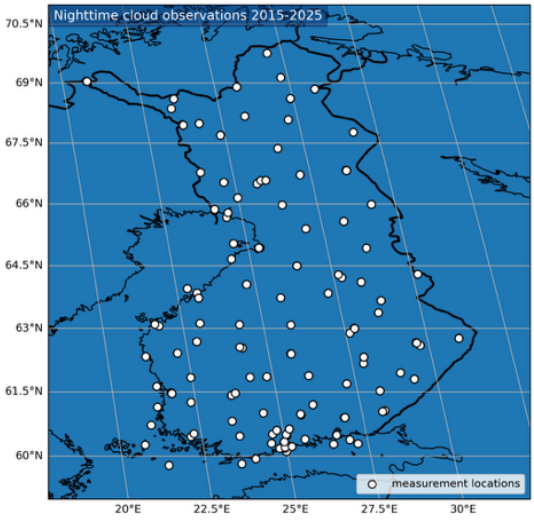

Figure B1. Locations of the cloud-okta-observing weather stations, based on FMI's open data cloud-okta measurements, within [20, 32]° E and [59, 71]° N.

However, we can statistically estimate the impact of the typical nighttime cloudiness on ground-based aurora observations by utilising the dense network of weather stations in the aurora observation region. With adequate temporal resolution and coverage of weather observations over one solar cycle, cloudiness observations can cover the typical times, period and area that influence the aurora observations. By averaging the cloudiness data into monthly bins, we mitigate spatio-temporal noise (e.g. topological or short-term cloud coverage difference between aurora and weather observations), enabling us to capture the general trend connecting the two types of observations from the same region (in our case, Finland). As a first-order approximation, one may expect that an increase in typical nighttime cloudiness should in turn decrease the typical amount of aurora observations recorded in Skywarden.

To estimate the impact of the typical monthly cloudiness on the aurora observations made in Finland, we calculate the monthly average nighttime cloudiness in Finland, between

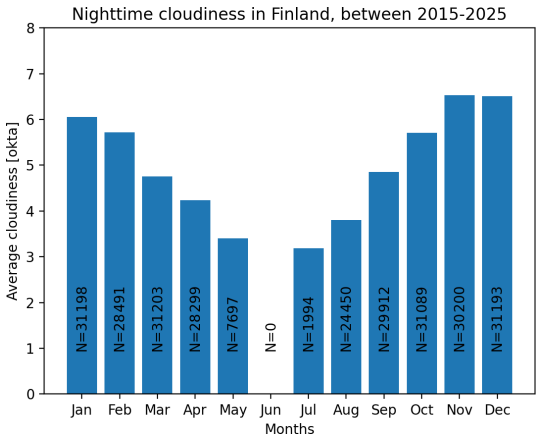

Figure B2. Average nighttime cloudiness in Finland (expressed in okta) based on the Finnish Meteorological Institute's open data hourly cloud-okta values, during 2015–2025. Nighttime hours are defined when the Sun's elevation is at least 10° below the horizon (i.e. solar zenith angle greater than 100°). The number of nighttime days contributing to a given month's statistics is indicated in the corresponding bar of the diagram.

years 2015–2025, using the Finnish Meteorological Institute (FMI)'s open data cloud-okta measurements. The FMI API (https://en.ilmatieteenlaitos.fi/open-data, last access: 25 August 2026) provides cloudiness measurements that comprise manual optical observations and automated ceilometer measurements (a map of FMI's ceilometer network can be found on http://ceilometer.fmi.fi/, last access: 25 August 2026). Ceilometers measure clouds up to 7.5 km altitude and identify four different cloud layers. The total cloudiness, expressed in okta on a scale from 0 (clear sky) to 8 (overcast), includes all cloud layers and is obtained from the last 30 min of observations.

To obtain the statistics of the nighttime cloudiness, we first retrieved the hourly weather data from the FMI API for each day during years 2015–2025, for all weather stations within latitudes comprised between 59 and 71° N and longitudes comprised between 20 and 32° E (see Fig. B1). Then, we retained the cloud-okta measurements corresponding to nighttime hours and calculated their daily average. Nighttime is defined as time when the solar elevation at ground level at a given meteorological station is at least 10° below the horizon (i.e. the solar zenith angle is greater than 100°). Once processed, we collected these cloud-okta values from each station into monthly bins and calculated averages within each bin. The resulting distribution of monthly average (over years and stations) nighttime cloudiness in Finland is shown in Fig. B2. Result do not change significantly if hourly (instead of daily) values are used before monthly binning. This is because the number of nighttime hours in a given month does not change much from a year to another one.

Appendix C: Parameter distributions and analysis restricted to observations from the European sector

To evaluate the robustness of the histograms presented in Figs. 3–6, we repeat the same analysis but restricting it to Skywarden observations from the European sector. The results are shown in Figs. C1–C4.

We also carry out the same assessment of statistical significance of the differences between all-aurora and dune histograms and summarise the results in Table C1.

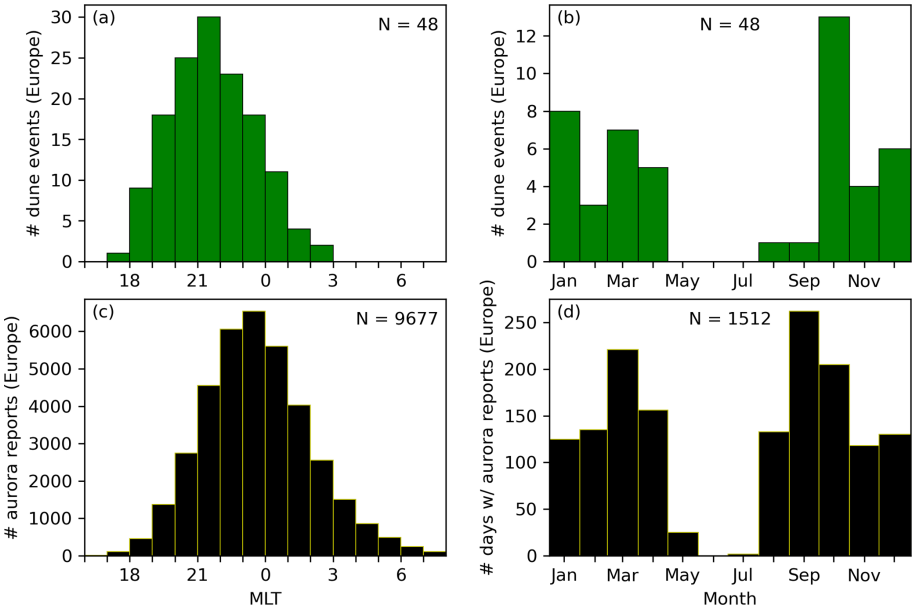

Figure C1. Same as Fig. 3 but considering only the Skywarden reports from the European sector.

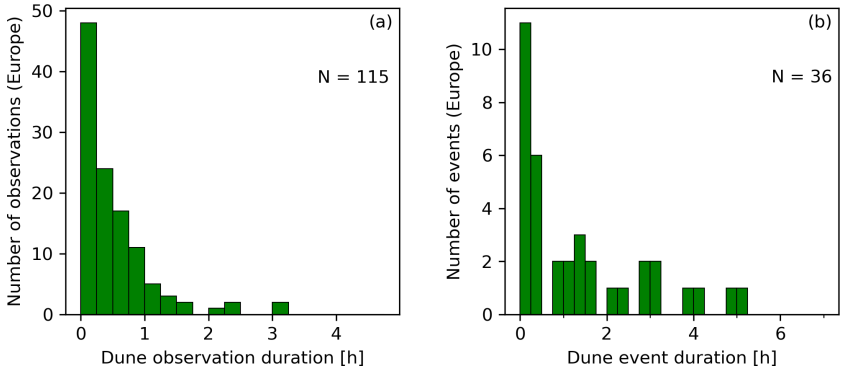

Figure C2. Same as Fig. 4 but considering only the Skywarden reports from the European sector.

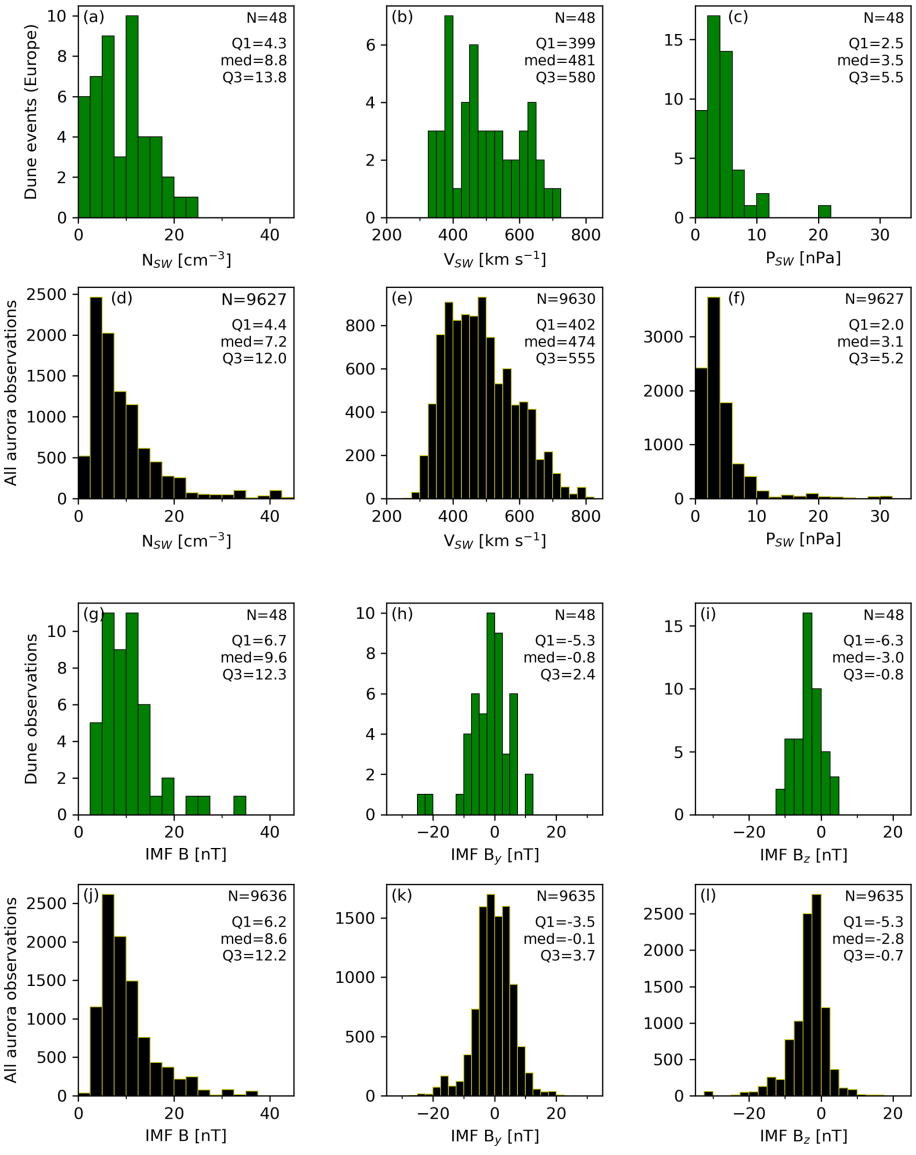

Figure C3. Same as Fig. 5 but considering only the Skywarden reports from the European sector.

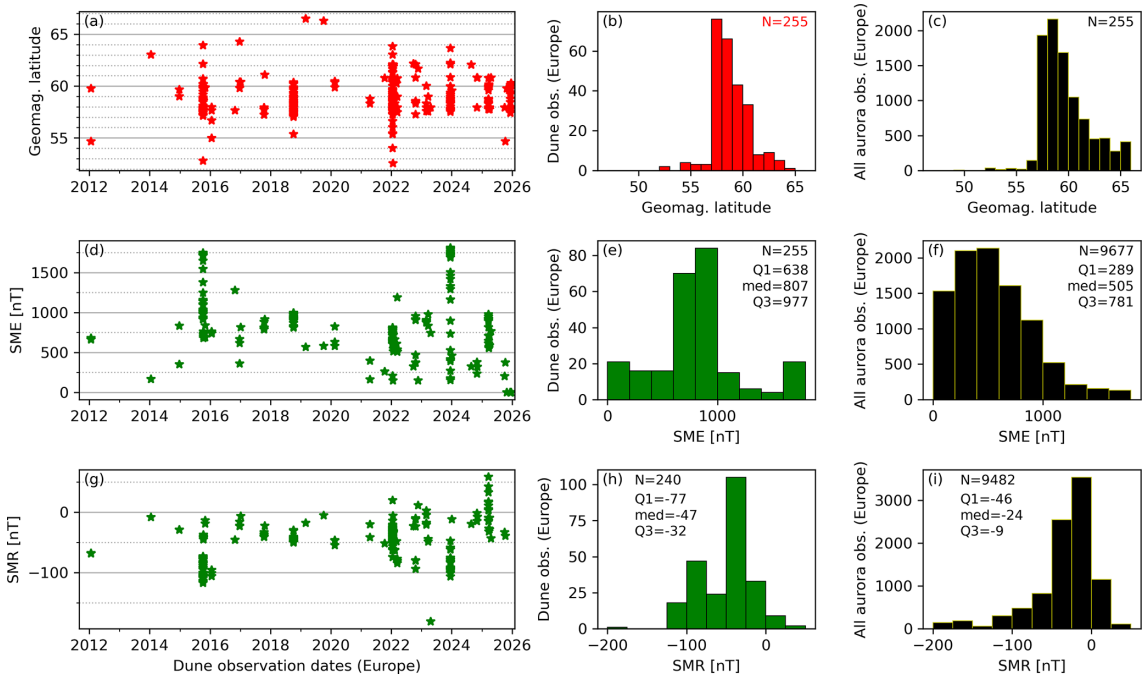

Figure C4. Same as Fig. 6 but considering only the Skywarden reports from the European sector.

Table C1. Evaluation of the statistical significance of the differences between the dune and all-aurora distributions shown in Figs. C1–C4. Differences are assessed using permutation tests (20 000 iterations) with false discovery rate (FDR) correction, similar to Table 1, but restricted to the Skywarden reports from the European sector.

Parameter	Effect size (statistic)	p-value	q-value	Significant (FDR 0.05)
MLT	2.0 h (circular mean)	$< 5 \times 10^{-5}$	0.00017	Yes
Monthly distribution	0.30 (TV)	0.00175	0.00437	Yes
SW density	1.5 cm^{-3} (median)	0.12984	0.25969	No
SW speed	7.8 $km\,s^{-1}$ (median)	0.68507	0.70461	No
SW pressure	0.43 nPa (median)	0.21299	0.32070	No
IMF $\lvert B \rvert$	1.0 nT (median)	0.22449	0.32070	No
IMF B_y	0.75 nT (median)	0.52652	0.65815	No
IMF B_z	0.23 nT (median)	0.70461	0.70461	No
SME	303 nT (median)	$< 5 \times 10^{-5}$	0.00017	Yes
SMR	22.4 nT (median)	$< 5 \times 10^{-5}$	0.00017	Yes

Data availability. The raw data used to set up the list of dune aurora observations between 1 January 2000 and 31 December 2025 were obtained from the Skywarden/Taivaanvahti API with the following command: https://www.taivaanvahti.fi/app/api/search.php?format=html&language=en&start=2000-01-01&end=2025-12-31&category=revontuli&detail_exact=dunes&with_images=1&columns=id,user,start_utc,city,latitude,longitude,details&format=csv (last access: 25 August 2026). The list of visually validated observations for the purpose of this study are available from https://doi.org/10.57707/fmi-b2share.0n576-3rb80 (Grandin and Bruus, 2026).

The list of all aurora observations in Skywarden/Taivaanvahti between 1 January 2000 until 31 December 2025 can be retrieved with the following command: https://www.taivaanvahti.fi/app/api/search.php?format=html&language=en&start=2000-01-01&end=2025-12-31&category=revontuli&columns=id,user,start_utc,end_utc,city,latitude,longitude,details&format=csv.

The OMNI data (Papitashvili and King, 2020) are available at https://doi.org/10.48322/1shr-ht18.

The SuperMAG magnetic index data (Gjerloev, 2012; Newell and Gjerloev, 2011, 2012) are available at https://supermag.jhuapl.edu (last access: 25 August 2026).

IMAGE data are available at https://space.fmi.fi/image/ (last access: 25 August 2026). The code for the SECS method is available as a supplement to Vanhamäki and Juusola (2020).

The cloudiness data across Finland for years 2015–2025 were obtained through the Finnish Meteorological Institute's open data API: https://en.ilmatieteenlaitos.fi/download-observations (last access: 25 August 2026).

Author contributions. MG designed the study, carried out most of the data analysis, and wrote most of the manuscript. LJ carried out the equivalent current analysis and contributed with text to Sects. 2.4 and 3.5. JR and EB carried out the statistical analysis of cloudiness in Finland presented in Appendix B (text by JR). DL provided the original photograph shown in Fig. 1. All co-authors have read the manuscript and provided comments to improve it.

Competing interests. The contact author has declared that none of the authors has any competing interests.

Disclaimer. Publisher's note: Copernicus Publications remains neutral with regard to jurisdictional claims made in the text, published maps, institutional affiliations, or any other geographical representation in this paper. The authors bear the ultimate responsibility for providing appropriate place names. Views expressed in the text are those of the authors and do not necessarily reflect the views of the publisher.

Acknowledgements. The authors wish to thank the 183 named and 4 anonymous citizen scientists who submitted dune observation reports to the Skywarden observation system (see the list of names in Appendix A). We also thank the Ursa Astronomical association for developing and maintaining Skywarden, as well as the moderators who check the submissions. MG expresses special thanks to Les Ladbrook (Aurora Australis (NZ)), Margaret Sonnermann (Aurora Australis Tasmania), Nick Bull (Aurora Hunters UK & Iceland), Donna Lach & Alysa Ferguson (Manitoba Aurora Chasers), and Tom Egil Dørum (Northern Lights (Nordlys) – https://www.nordlysvarsel.com, last access: 25 August 2026) for sharing the call to report dune aurora observations to Skywarden via the aurora chaser Facebook groups they are administrating.

We thank the institutes who maintain the IMAGE Magnetometer Array: Tromsø Geophysical Observatory of UiT the Arctic University of Norway (Norway), Finnish Meteorological Institute (Finland), Institute of Geophysics Polish Academy of Sciences (Poland), GFZ German Research Centre for Geosciences (Germany), Geological Survey of Sweden (Sweden), Swedish Institute of Space Physics (Sweden), Sodankylä Geophysical Observatory of the University of Oulu (Finland), DTU Technical University of Denmark (Denmark), and Science Institute of the University of Iceland (Iceland). The provisioning of data from AAL, GOT, HAS, NRA, VXJ, FKP, ROE, BFE, BOR, HOV, SCO, KUL, and NAQ is supported by the ESA contracts number 4000128139/19/D/CT as well as 4000138064/22/D/KS.

This research was supported by the International Space Science Institute (ISSI) in Bern, Switzerland, through ISSI Working Group project ARCTICS (https://collab.issibern.ch/arctics/; last access: 25 August 2026). We gratefully acknowledge the SuperMAG collaborators (http://supermag.jhuapl.edu/info/?page=acknowledgement, last access: 25 August 2026). We acknowledge use of NASA/GSFC's Space Physics Data Facility's OMNIWeb service, and OMNI data. The Scientific colour maps `turku` and `romaO` (Crameri, 2023) are used in this study to prevent visual distortion of the data and exclusion of readers with colour-vision deficiencies (Crameri et al., 2020).

MG acknowledges funding from the Research Council of Finland (grant 360433-ANAON) and from the European Union (ERC Starting Grant, LOUARN, 101161971). Views and opinions expressed are however those of the authors only and do not necessarily reflect those of the European Union or the European Research Council. Neither the European Union nor the granting authority can be held responsible for them. EB wishes to thank the Research Council of Finland for the support through grant 365202. EK acknowledges the Magnus Ehrnrooth Foundation for a travel grant to attend the ISSI meetings in Bern on 3–7 June 2024 and on 5–9 May 2025, and DL thanks the University of Calgary for the travel support to attend these meetings.

Financial support. This research has been supported by the HORIZON EUROPE European Research Council (grant no. 101161971-LOUARN), the Research Council of Finland (grant nos. 360433-ANAON and 365202), the Magnus Ehrnroothin Säätiö (Eero Karvinen travel grant, 2024), and the International Space Science Institute (ARCTICS).

Review statement. This paper was edited by Dalia Buresova and reviewed by two anonymous referees.

References

Amm, O.: Ionospheric Elementary Current Systems in Spherical Coordinates and Their Application, J. Geomagn. Geoelectr., 49, 947–955, https://doi.org/10.5636/jgg.49.947, 1997.

Archer, W. E., Gallardo-Lacourt, B., Perry, G. W., St. -Maurice, J. P., Buchert, S. C., and Donovan, E.: Steve: The Optical Signature of Intense Subauroral Ion Drifts, Geophys. Res. Lett., 46, 6279–6286, https://doi.org/10.1029/2019GL082687, 2019.

Beldon, C. L. and Mitchell, N. J.: Gravity wave-tidal interactions in the mesosphere and lower thermosphere over Rothera, Antarctica (68° S, 68°W), J. Geophys. Res.-Atmos., 115, D18101, https://doi.org/10.1029/2009JD013617, 2010.

Benjamini, Y. and Hochberg, Y.: Controlling the false discovery rate: a practical and powerful approach to multiple testing, J. R. Stat. Soc. B, 57, 289–300, https://doi.org/10.1111/j.2517-6161.1995.tb02031.x, 1995.

Brown, L. B., Gerrard, A. J., Meriwether, J. W., and Makela, J. J.: All-sky imaging observations of mesospheric fronts in OI 557.7 nm and broadband OH airglow emissions: Analysis of frontal structure, atmospheric background conditions, and potential sourcing mechanisms, J. Geophys. Res.-Atmos., 109, D19104, https://doi.org/10.1029/2003JD004223, 2004.

Bruus, E.: Taivaanvahti/Himlakollen/Skywatcher's search interface, https://www.taivaanvahti.fi/app/docs/interface/output_interface_en.html, (last access: 24 August 2026), 2024.

Burrell, A., van der Meeren, C., and Laundal, K. M.: aburrell/aacgmv2: Version 2.6.0, Zenodo [software], https://doi.org/10.5281/zenodo.3598705, 2020.

Chauhan, N., Shiokawa, K., Gurubaran, S., Nozawa, S., Oyama, S.-I., and Nakamura, T.: Occurrence of Mesospheric Frontal Structures Over the High Latitude Station, Tromsø, Norway, J. Geophys. Res.-Space, 129, e2023JA032243, https://doi.org/10.1029/2023JA032243, 2024.

Crameri, F.: Scientific colour maps v8.0.1, Zenodo [software], https://doi.org/10.5281/zenodo.8409685, 2023.

Crameri, F., Shephard, G. E., and Heron, P. J.: The misuse of colour in science communication, Nat. Commun., 11, 5444, https://doi.org/10.1038/s41467-020-19160-7, 2020.

de Wit, R. J., Hibbins, R. E., and Espy, P. J.: The seasonal cycle of gravity wave momentum flux and forcing in the high latitude northern hemisphere mesopause region, J. Atmos. Sol.-Terr. Phy., 127, 21–29, https://doi.org/10.1016/j.jastp.2014.10.002, 2015.

Dewan, E. M. and Picard, R. H.: Mesospheric bores, J. Geophys. Res., 103, 6295–6306, https://doi.org/10.1029/97JD02498, 1998.

Dewan, E. M. and Picard, R. H.: On the origin of mesospheric bores, J. Geophys. Res., 106, 2921–2927, https://doi.org/10.1029/2000JD900697, 2001.

Fritts, D. C. and Alexander, M. J.: Gravity wave dynamics and effects in the middle atmosphere, Rev. Geophys., 41, 1003, https://doi.org/10.1029/2001RG000106, 2003.

Garcia, R. R. and Solomon, S.: The effect of breaking gravity waves on the dynamics and chemical composition of the mesosphere and lower thermosphere, J. Geophys. Res.-Atmos., 90, 3850–3868, https://doi.org/10.1029/JD090iD02p03850, 1985.

Gjerloev, J. W.: The SuperMAG data processing technique, J. Geophys. Res.-Space, 117, A09213, https://doi.org/10.1029/2012JA017683, 2012.

Gonzalez, W. D., Joselyn, J. A., Kamide, Y., Kroehl, H. W., Rostoker, G., Tsurutani, B. T., and Vasyliunas, V. M.: What is a geomagnetic storm?, J. Geophys. Res., 99, 5771–5792, https://doi.org/10.1029/93JA02867, 1994.

Grandin, M. and Bruus, E.: Visually validated dune aurora observations from Skywarden between 2000 and 2025, FMI Research Data Repository METIS [data set], https://doi.org/10.57707/fmi-b2share.0n576-3rb80, 2026.

Grandin, M., Palmroth, M., Whipps, G., Kalliokoski, M., Ferrier, M., Paxton, L. J., Mlynczak, M. G., Hilska, J., Holmseth, K., Vinorum, K., and Whenman, B.: Large-Scale Dune Aurora Event Investigation Combining Citizen Scientists' Photographs and Spacecraft Observations, AGU Advances, 2, e00338, https://doi.org/10.1029/2020AV000338, 2021.

Grandin, M., Bruus, E., Ledvina, V. E., Partamies, N., Barthelemy, M., Martinis, C., Dayton-Oxland, R., Gallardo-Lacourt, B., Nishimura, Y., Herlingshaw, K., Thomas, N., Karvinen, E., Lach, D., Spijkers, M., and Bergstrand, C.: The Gannon Storm: citizen science observations during the geomagnetic superstorm of 10 May 2024, Geosci. Commun., 7, 297–316, https://doi.org/10.5194/gc-7-297-2024, 2024.

Grandin, M., Ledvina, V. E., Musset, S., Partamies, N., Frissell, N. A., Bruus, E., Nicoll, K. A., Mkrtchyan, H., Gallardo-Lacourt, B., Alfonsi, L., Jonassen, M. O., Whiter, D., Herlingshaw, K., Enengl, F., Doornbos, E., Jia, J., Kosar, B., Evans, L. P., Haberle, V., Laundal, K. M., and Barthelemy, M.: Citizen Science in Space and Atmospheric Sciences: Opportunities and Challenges, Surv. Geophys., https://doi.org/10.1007/s10712-025-09888-6, 2025.

Hayakawa, H., Ebihara, Y., Mishev, A., Koldobskiy, S., Kusano, K., Bechet, S., Yashiro, S., Iwai, K., Shinbori, A., Mursula, K., Miyake, F., Shiota, D., Silveira, M. V. D., Stuart, R., Oliveira, D. M., Akiyama, S., Ohnishi, K., Ledvina, V., and Miyoshi, Y.: The Solar and Geomagnetic Storms in 2024 May: A Flash Data Report, Astrophys. J., 979, 49, https://doi.org/10.3847/1538-4357/ad9335, 2025.

He, F., Yao, Z., Ni, B., Cao, X., Ye, S., Guo, R., Li, J., Ren, Z., Yue, X., Zhang, Y., Wei, Y., Zhang, X., and Pu, Z.: Sawtooth and dune auroras simultaneously driven by waves around the plasmapause, Earth and Planetary Physics, 7, 237–246, https://doi.org/10.26464/epp2023023, 2023.

Heelis, R. A. and Maute, A.: Challenges to Understanding the Earth's Ionosphere and Thermosphere, J. Geophys. Res.-Space, 125, e27497, https://doi.org/10.1029/2019JA027497, 2020.

Herlingshaw, K., Lach, D., Dayton-Oxland, R., Bruus, E., Karvinen, E., Ledvina, V., Partamies, N., Grandin, M., Spijkers, M., Nishimura, Y., Knudsen, D., Ladbrook, L., Martinis, C., Gallardo-Lacourt, B., Dyer, A., Mielke, L., Ratzlaff, C., Evans, L., Helin, M., Kuzub, J., Barthelemy, M., Thomas, N., Glad, M., Donovan, E., Syrjäsuo, M., Cordon, S., Andersen, J., and Legg, C.: ARCTICS Aurora Field Guide and Handbook for Citizen Science, Zenodo, https://doi.org/10.5281/zenodo.13931939, 2024.

Hozumi, Y., Saito, A., Sakanoi, T., Yamazaki, A., Hosokawa, K., and Nakamura, T.: Geographical and Seasonal Variability of Mesospheric Bores Observed from the International Space Station, J. Geophys. Res.-Space, 124, 3775–3785, https://doi.org/10.1029/2019JA026635, 2019.

Izvekova, Y. N., Popel, S. I., Morozova, T. I., and Kopnin, S. I.: Possible manifestation of dusty ionospheric plas-

mas during high-speed meteor showers, Icarus, 429, 116383, https://doi.org/10.1016/j.icarus.2024.116383, 2025.

King, J. H. and Papitashvili, N. E.: Solar wind spatial scales in and comparisons of hourly Wind and ACE plasma and magnetic field data, J. Geophys. Res.-Space, 110, 2104, https://doi.org/10.1029/2004JA010649, 2005.

Kosar, B. C., MacDonald, E. A., Case, N. A., and Heavner, M.: Aurorasaurus Database of Real-Time, Crowd-Sourced Aurora Data for Space Weather Research, Earth and Space Science, 5, 970–980, https://doi.org/10.1029/2018EA000454, 2018.

Kumar, A., Stolle, C., Yamazaki, Y., Pedatella, N. M., Kunze, M., Stephan, C. C., Siddiqui, T. A., and Sunil Krishna, M. V.: Impact of Weak and Strong Stratospheric Polar Vortices in the Northern and Southern Hemispheres on Solar-Migrating Semidiurnal Tides in UA-ICON, J. Geophys. Res.-Atmos., 130, e2025JD043550, https://doi.org/10.1029/2025JD043550, 2025.

Lockwood, M., Owens, M. J., Brown, W., and Vázquez, M.: The 2024 May event in the context of auroral activity over the past 375 yr, Mon. Not. R. Astron. Soc., 540, 3596–3624, https://doi.org/10.1093/mnras/staf827, 2025.

MacDonald, E. A., Case, N. A., Clayton, J. H., Hall, M. K., Heavner, M., Lalone, N., Patel, K. G., and Tapia, A.: Aurorasaurus: A citizen science platform for viewing and reporting the aurora, Space Weather, 13, 548–559, https://doi.org/10.1002/2015SW001214, 2015.

MacDonald, E. A., Donovan, E., Nishimura, Y., Case, N. A., Gillies, D. M., Gallardo-Lacourt, B., Archer, W. E., Spanswick, E. L., Bourassa, N., Connors, M., Heavner, M., Jackel, B., Kosar, B., Knudsen, D. J., Ratzlaff, C., and Schofield, I.: New science in plain sight: Citizen scientists lead to the discovery of optical structure in the upper atmosphere, Sci. Adv., 4, eaaq0030, https://doi.org/10.1126/sciadv.aaq0030, 2018.

Nevanlinna, H. and Tanskanen, E. I.: Early auroral photography and observations at the Sodankylä Geophysical Observatory in Finland, 1927–1929, Hist. Geo Space. Sci., 15, 17–25, https://doi.org/10.5194/hgss-15-17-2024, 2024.

Newell, P. T. and Gjerloev, J. W.: Evaluation of SuperMAG auroral electrojet indices as indicators of substorms and auroral power, J. Geophys. Res.-Space, 116, A12211, https://doi.org/10.1029/2011JA016779, 2011.

Newell, P. T. and Gjerloev, J. W.: SuperMAG-based partial ring current indices, J. Geophys. Res.-Space, 117, A05215, https://doi.org/10.1029/2012JA017586, 2012.

Nishimura, Y., Bruus, E., Karvinen, E., Martinis, C. R., Dyer, A., Kangas, L., Rikala, H. K., Donovan, E. F., Nishitani, N., and Ruohoniemi, J. M.: Interaction Between Proton Aurora and Stable Auroral Red Arcs Unveiled by Citizen Scientist Photographs, J. Geophys. Res.-Space, 127, e30570, https://doi.org/10.1029/2022JA030570, 2022.

Nitta, N. V., Mulligan, T., Kilpua, E. K. J., Lynch, B. J., Mierla, M., O'Kane, J., Pagano, P., Palmerio, E., Pomoell, J., Richardson, I. G., Rodriguez, L., Rouillard, A. P., Sinha, S., Srivastava, N., Talpeanu, D.-C., Yardley, S. L., and Zhukov, A. N.: Understanding the Origins of Problem Geomagnetic Storms Associated with "Stealth" Coronal Mass Ejections, Space Sci. Rev., 217, 82, https://doi.org/10.1007/s11214-021-00857-0, 2021.

Ono, T., Hirasawa, T., and Meng, C. I.: Proton auroras observed at the equatorward edge of the duskside auroral oval, Geophys. Res. Lett., 14, 660–663, https://doi.org/10.1029/GL014i006p00660, 1987.

Palmroth, M., Grandin, M., Helin, M., Koski, P., Oksanen, A., Glad, M. A., Valonen, R., Saari, K., Bruus, E., Norberg, J., Viljanen, A., Kauristie, K., and Verronen, P. T.: Citizen Scientists Discover a New Auroral Form: Dunes Provide Insight Into the Upper Atmosphere, AGU Advances, 1, e00133, https://doi.org/10.1029/2019AV000133, 2020.

Palmroth, M., Grandin, M., Sarris, T., Doornbos, E., Tourgaidis, S., Aikio, A., Buchert, S., Clilverd, M. A., Dandouras, I., Heelis, R., Hoffmann, A., Ivchenko, N., Kervalishvili, G., Knudsen, D. J., Kotova, A., Liu, H.-L., Malaspina, D. M., March, G., Marchaudon, A., Marghitu, O., Matsuo, T., Miloch, W. J., Moretto-Jørgensen, T., Mpaloukidis, D., Olsen, N., Papadakis, K., Pfaff, R., Pirnaris, P., Siemes, C., Stolle, C., Suni, J., van den IJssel, J., Verronen, P. T., Visser, P., and Yamauchi, M.: Lower-thermosphere–ionosphere (LTI) quantities: current status of measuring techniques and models, Ann. Geophys., 39, 189–237, https://doi.org/10.5194/angeo-39-189-2021, 2021.

Papitashvili, N. E. and King, J. H.: OMNI Hourly Data, NASA Space Physics Data Facility [data set], https://doi.org/10.48322/1shr-ht18, 2020.

Pitkänen, T., Hamrin, M., Kullen, A., Maggiolo, R., Karlsson, T., Nilsson, H., and Norqvist, P.: Response of magnetotail twisting to variations in IMF B_y: A THEMIS case study 1-2 January 2009, Geophys. Res. Lett., 43, 7822–7830, https://doi.org/10.1002/2016GL070068, 2016.

Rong, Z. J., Lui, A. T. Y., Wan, W. X., Yang, Y. Y., Shen, C., Petrukovich, A. A., Zhang, Y. C., Zhang, T. L., and Wei, Y.: Time delay of interplanetary magnetic field penetration into Earth's magnetotail, J. Geophys. Res.-Space, 120, 3406–3414, https://doi.org/10.1002/2014JA020452, 2015.

Russell, C. T. and McPherron, R. L.: Semiannual variation of geomagnetic activity, J. Geophys. Res., 78, 92, https://doi.org/10.1029/JA078i001p00092, 1973.

Sarris, T., Palmroth, M., Aikio, A., Buchert, S. C., Clemmons, J., Clilverd, M., Dandouras, I., Doornbos, E., Goodwin, L. V., Grandin, M., Heelis, R., Ivchenko, N., Moretto-Jørgensen, T., Kervalishvili, G., Knudsen, D., Liu, H.-L., Lu, G., Malaspina, D. M., Marghitu, O., Maute, A., Miloch, W. J., Olsen, N., Pfaff, R., Stolle, C., Talaat, E., Thayer, J., Tourgaidis, S., Verronen, P. T., and Yamauchi, M.: Plasma-Neutral Interactions in the Lower Thermosphere-Ionosphere: The need for in situ measurements to address focused questions, Frontiers in Astronomy and Space Sciences, 9, 435, https://doi.org/10.3389/fspas.2022.1063190, 2023.

Seltveit, S. H.: Auroral dunes: Bores or boring? Airglow imaging of gravity wave–aurora interaction in the mesosphere lower thermosphere, Master's thesis, NTNU – Norwegian University of Science and Technology, Trondheim, Norway, https://hdl.handle.net/11250/3033754, 2022.

Shepherd, S. G.: Altitude-adjusted corrected geomagnetic coordinates: Definition and functional approximations, J. Geophys. Res.-Space, 119, 7501–7521, https://doi.org/10.1002/2014JA020264, 2014.

Smith, S. M., Taylor, M. J., Swenson, G. R., She, C.-Y., Hocking, W., Baumgardner, J., and Mendillo, M.: A multidiagnostic investigation of the mesospheric bore phenomenon, J. Geophys. Res.-Space, 108, 1083, https://doi.org/10.1029/2002JA009500, 2003.

Spogli, L., Alberti, T., Bagiacchi, P., Cafarella, L., Cesaroni, C., Cianchini, G., Coco, I., Di Mauro, D., Ghidoni, R., Giannattasio, F., Ippolito, A., Marcocci, C., Pezzopane, M., Pica, E., Pignalberi, A., Perrone, L., Romano, V., Sabbagh, D., Scotto, C., Spadoni, S., Tozzi, R., and Viola, M.: The effects of the May 2024 Mother's Day superstorm over the Mediterranean sector: from data to public communication, Ann. Geophys., 67, PA218, https://doi.org/10.4401/ag-9117, 2024.

Storey, J. D.: A Direct Approach to False Discovery Rates, J. R. Stat. Soc. B, 64, 479–498, https://doi.org/10.1111/1467-9868.00346, 2002.

Su, Y., Yue, J., Liu, X., Miller, S. D., Straka III, W. C., Smith, S. M., Guo, D., and Guo, S.: Mesospheric Bore Observations Using Suomi-NPP VIIRS DNB during 2013-2017, Remote Sens., 10, 1935, https://doi.org/10.3390/rs10121935, 2018.

Vadas, S. L. and Becker, E.: Numerical Modeling of the Generation of Tertiary Gravity Waves in the Mesosphere and Thermosphere During Strong Mountain Wave Events Over the Southern Andes, J. Geophys. Res.-Space, 124, 7687–7718, https://doi.org/10.1029/2019JA026694, 2019.

Vadas, S. L. and Liu, H.-L.: Generation of large-scale gravity waves and neutral winds in the thermosphere from the dissipation of convectively generated gravity waves, J. Geophys. Res.-Space, 114, A10310, https://doi.org/10.1029/2009JA014108, 2009.

Vanhamäki, H. and Juusola, L.: Introduction to Spherical Elementary Current Systems, in: Ionospheric Multi-Spacecraft Analysis Tools, ISSI Scientific Report Series 17, 5–33, https://doi.org/10.1007/978-3-030-26732-2_13, 2020.

Weygand, J. M. and Wing, S.: Comparison of DMSP and SECS region-1 and region-2 ionospheric current boundary, J. Atmos. Sol.-Terr. Phy., 143–144, 8–13, https://doi.org/10.1016/j.jastp.2016.03.002, 2016.

Zhang, Y., Sun, W., Feng, X. S., Deehr, C. S., Fry, C. D., and Dryer, M.: Statistical analysis of corotating interaction regions and their geoeffectiveness during solar cycle 23, J. Geophys. Res.-Space, 113, A08106, https://doi.org/10.1029/2008JA013095, 2008.